RNA interference assay. siRNA was synthesized chemically at Hokkaido System Science. The sequences of siRNA oligonucleotides were as follows: Tax, 5′-GGCCUUAUUUGGACAUUUATT-3′ and 5′-UAAAUGUCCAAAUAAGGCCTT-3′ (31); Luc, 5′-CGUACGCG-GAAUACUUCGATT-3′ and 5′-UCGAAGUAUUCCGCGUACGTT3′. Next, 100 pmol annealed RNA duplex was transfected using Human T cell Amaxa Nucleofector Kit according to the manufacturer's recommendations (Lonza). 100 pmol Luc siRNA was used as a negative control. Cells were incubated for 48 hours and then harvested and subjected to real-time RT-PCR analysis.

Measurement of IFN-γ. IFN-γ concentration in the culture supernatant was measured with a cytometric bead array kit (BD Biosciences) using a FACSCalibur flow cytometer (BD Biosciences) according to the manufacturer's instructions.

IP. Approximately 1 mg of MT-2 nuclear extracts were incubated with 5 μg anti-Tax, anti-Sp1, or normal IgG coupled with protein G–agarose (Roche Applied Science) in IP buffer (10 mM HEPES [pH 7.9], 100 mM KCl, 1 mM EDTA, 1 mM dithiothreitol, 0.1% NP-40, 1 mM Na_3VO_4, 5 mM NaF, 2 μg/ml aprotinin, 2 μg/ml leupeptin, and 2 μg/ml pepstatin) for 2 hours. The precipitated proteins were washed with the IP buffer, separated by 10% SDS-PAGE, and immunoblotted with anti-Tax or anti-Sp1 antibodies.

ChIP assay. ChIP assay was performed using a ChIP assay kit (Upstate Biotechnology) with some modifications. Briefly, 5×10^6 MT-2 cells were fixed with 1% formaldehyde at 37°C for 25 minutes and washed twice with PBS. Cells were subsequently harvested and sonicated in lysis buffer. Precleared chromatin samples were immunoprecipitated with 5 μg anti-Tax antibody, anti-Sp1 antibody, or normal IgG for 16 hours at 4°C. Immune complexes were collected with salmon sperm DNA/protein G–sepharose for 90 minutes with rotation, washed, and then incubated at 65°C for 6 hours for reverse cross-linking. Chromatin DNA was extracted and analyzed using PCR with primers for the *TBX21* promoter region (–179 to –59; forward, 5′-GCCAAGAGCGTAGAATTTGC-3′; reverse, 5′-CGCTTT-GCTGTGGCTTTATG-3′) (25, 61). Amplification was performed using ExTaq (Takara Bio) with 1 cycle at 95°C for 5 minutes followed by 30 cycles of 95°C for 30 seconds, 54°C for 30 seconds, and 72°C for 30 seconds. Amplified products were analyzed using 8% polyacrylamide gel electrophoresis.

Luciferase assay. For transient transfection, HEK293 cells were seeded at 5×10^4 cells/well into 24-well plates. After 12 hours, medium was changed to MEM supplemented with 10% FBS and 1% P/S, and each plasmid was transfected with CellPhect Transfection Kit according to the manufacturer's recommendations (GE Healthcare). 50 ng pRSV-βgal plasmid was included in each transfection experiment to control for the efficiency of transfection. The total amount of transfected DNA was kept constant with pcDNA3 in all samples. After 48 hours, cells were lysed with Passive Lysis Buffer (Promega), and luciferase activity was measured using the Promega luciferase assay system and MicroLumat Plus LB96V (Berthold Technologies). Values were normalized to β-galactosidase activity as an internal control.

Tissue staining. Formalin-fixed thoracic spinal cord tissue sections were deparaffinized in xylene and rehydrated in a series of graded alcohols and distilled water. The antigenicity of the tissue sections was recovered using a standard microwave heating technique. For immunofluorescence, the slides were incubated in PBS with 10% goat serum for 1 hour at room temperature, then in anti-CCR4 antibody, anti–T-bet antibody, anti–IFN-γ antibody, and anti-CXCR3 antibody overnight at 4°C, labeled with Alexa Fluor 488– or Alexa Fluor 594–conjugated secondary antibody, and examined under a fluorescence microscope (Nikon eclipse E600 with fluorescence filter Nikon F-FL; Nikon Instech) with rabbit or goat IgG as the negative control. Tissue sections were also stained with H&E.

Immunofluorescence staining and immunofluorescence-FISH. Jurkat cells, MT-2 cells, and cells from the CSF of 3 HAM/TSP patients were attached to slides using a cytospin centrifuge (Thermo Fisher Scientific) and fixed in 4% paraformaldehyde (Wako Pure Chemical Industries) for 30 minutes. The slides were washed with PBS and then pretreated as follows: slides were immersed in room temperature 0.2M HCl for 20 minutes, followed by 0.2% Triton-X/PBS for 10 minutes, and finally 0.005% pepsin/0.1M HCl heated to 37°C for 5 minutes. After pretreatment, the slides were stained using the immunofluorescence Can Get Signal kit (TOYOBO) according the manufacturer's instructions with anti-CCR4 as the primary antibody and Alexa Fluor 488–conjugated anti-goat IgG as the secondary antibody. After again being fixed with 4% paraformaldehyde, cells were incubated with a nick-translated (Spectrum Red) pUC/HTLV-1 DNA probe, first for 5 minutes at 70°C and then overnight at 37°C. Images were obtained under an automated research microscope (Leica DMRA2) and analyzed with CW4000 FISH software (Leica Microsystems).

Proliferation assay. PBMCs from HAM/TSP patients were plated into 96-well round-bottomed plates (1×10^5 cells/well) and cultured without any mitogenic stimuli. Cell proliferation was measured using a ^{3}H-thymidine incorporation assay as described previously (19).

Statistics. Paired 2-tailed Student's *t* test and Wilcoxon test were used for within-group comparisons. Unpaired 2-tailed Student's *t* test or Mann-Whitney *U* test was used for between-group comparisons. 1-way ANOVA was used for multiple comparisons, followed by Dunnett or Tukey test. Friedman test was used for paired multiple comparisons, followed by Dunn test. Statistical analyses were performed using Graphpad Prism 5 (GraphPad Software Inc.). A *P* value less than 0.05 was considered significant.

Study approval. Written informed consent was obtained from all patients before the study, which was reviewed and approved by the Institutional Ethics Committee at St. Marianna University and conducted in compliance with the tenets of the Declaration of Helsinki.

Acknowledgments

The authors acknowledge the excellent technical assistance provided by Yumiko Hasegawa, M. Koike, Y. Suzuki-Ishikura, and Y. Saito. This work was partly supported by project "Research on Measures for Intractable Disease"; by a matching fund subsidy from the Ministry of Health Labour and Welfare; by JSPS KAKENHI grant nos. 24790898, 25461294, and 25461293; by the Takeda Science Foundation; and by the Daiichi Sankyo Foundation of Life Science.

Address correspondence to: Yoshihisa Yamano, Department of Rare Diseases Research, Institute of Medical Science, St. Marianna University School of Medicine, 2-16-1 Sugao, Miyamae-ku, Kanagawa 216-8512, Japan. Phone: 81.44.977.8111; E-mail: yyamano@marianna-u.ac.jp.

1. Murphy KM, Stockinger B. Effector T cell plasticity: flexibility in the face of changing circumstances. *Nat Immunol*. 2010;11(8):674–680.
2. Cosmi L, Maggi L, Santarlasci V, Liotta F, Annunziato F. T helper cells plasticity in inflammation. *Cytometry A*. 2014;85(1):36–42.
3. Long SA, Buckner JH. CD4+FOXP3+ T regulatory cells in human autoimmunity: more than a numbers game. *J Immunol*. 2011;187(5):2061–2066.
4. Zhou X, Bailey-Bucktrout S, Jeker LT, Bluestone JA. Plasticity of CD4(+) FoxP3(+) T cells. *Curr Opin Immunol*. 2009;21(3):281–285.
5. Hori S, Nomura T, Sakaguchi S. Control of regulatory T cell development by the transcription factor Foxp3. *Science*. 2003;299(5609):1057–1061.
6. Zhu J, Paul WE. CD4 T cells: fates, functions, and faults. *Blood*. 2008;112(5):1557–1569.
7. Ishida T, Ueda R. Immunopathogenesis of lymphoma: focus on CCR4. *Cancer Sci*. 2011;102(1):44–50.
8. Finney OC, Riley EM, Walther M. Phenotypic analysis of human peripheral blood regulatory T cells (CD4+FOXP3+CD127lo/–) ex vivo and after in vitro restimulation with malaria antigens. *Eur J Immunol*. 2010;40(1):47–60.
9. Mjosberg J, Berg G, Jenmalm MC, Ernerudh J. FOXP3+ regulatory T cells and T helper 1, T helper 2, and T helper 17 cells in human early pregnancy decidua. *Biol Reprod*. 2010;82(4):698–705.
10. Williams LM, Rudensky AY. Maintenance of the Foxp3-dependent developmental program in mature regulatory T cells requires continued expression of Foxp3. *Nat Immunol*. 2007;8(3):277–284.
11. Bennett CL, et al. The immune dysregulation, polyendocrinopathy, enteropathy, X-linked syndrome (IPEX) is caused by mutations of FOXP3. *Nat Genet*. 2001;27(1):20–21.
12. Gao Y, et al. Molecular mechanisms underlying the regulation and functional plasticity of FOXP3(+) regulatory T cells. *Genes Immun*. 2012;13(1):1–13.
13. Dominguez-Villar M, Baecher-Allan CM, Hafler DA. Identification of T helper type 1-like, Foxp3+ regulatory T cells in human autoimmune disease. *Nat Med*. 2011;17(6):673–675.
14. Sakaguchi S, et al. Foxp3+ CD25+ CD4+ natural regulatory T cells in dominant self-tolerance and autoimmune disease. *Immunol Rev*. 2006;212:8–27.
15. Viglietta V, Baecher-Allan C, Weiner HL, Hafler DA. Loss of functional suppression by CD4+CD25+ regulatory T cells in patients with multiple sclerosis. *J Exp Med*. 2004;199(7):971–979.
16. Kanangat S, et al. Disease in the scurfy (sf) mouse is associated with overexpression of cytokine genes. *Eur J Immunol*. 1996;26(1):161–165.
17. Lyon MF, Peters J, Glenister PH, Ball S, Wright E. The scurfy mouse mutant has previously unrecognized hematological abnormalities and resembles Wiskott-Aldrich syndrome. *Proc Natl Acad Sci U S A*. 1990;87(7):2433–2437.
18. Clark LB, Appleby MW, Brunkow ME, Wilkinson JE, Ziegler SF, Ramsdell F. Cellular and molecular characterization of the scurfy mouse mutant. *J Immunol*. 1999;162(5):2546–2554.
19. Yamano Y, et al. Abnormally high levels of virus-infected IFN-γ+ CCR4+ CD4+ CD25+ T cells in a retrovirus-associated neuroinflammatory disorder. *PLoS One*. 2009;4(8):e6517.
20. Yamano Y, et al. Virus-induced dysfunction of CD4+CD25+ T cells in patients with HTLV-I-associated neuroimmunological disease. *J Clin Invest*. 2005;115(5):1361–1368.
21. Niwa R, et al. Defucosylated chimeric anti-CC chemokine receptor 4 IgG1 with enhanced antibody-dependent cellular cytotoxicity shows potent therapeutic activity to T-cell leukemia and lymphoma. *Cancer Res*. 2004;64(6):2127–2133.
22. Yoshida M, Seiki M, Yamaguchi K, Takatsuki K. Monoclonal integration of human T-cell leukemia provirus in all primary tumors of adult T-cell leukemia suggests causative role of human T-cell leukemia virus in the disease. *Proc Natl Acad Sci U S A*. 1984;81(8):2534–2537.
23. Cook LB, Rowan AG, Melamed A, Taylor GP, Bangham CR. HTLV-1-infected T cells contain a single integrated provirus in natural infection. *Blood*. 2012;120(17):3488–3490.
24. Zhang L, Zhi H, Liu M, Kuo YL, Giam CZ. Induction of p21(CIP1/WAF1) expression by human T-lymphotropic virus type 1 Tax requires transcriptional activation and mRNA stabilization. *Retrovirology*. 2009;6:35.
25. Yu J, et al. Transcriptional control of human T-BET expression: the role of Sp1. *Eur J Immunol*. 2007;37(9):2549–2561.
26. Araya N, et al. Human T-lymphotropic virus type 1 (HTLV-1) and regulatory T cells in HTLV-1-associated neuroinflammatory disease. *Viruses*. 2011;3(9):1532–1548.
27. Ando H, et al. Positive feedback loop via astrocytes causes chronic inflammation in virus-associated myelopathy. *Brain*. 2013; 136(pt 9):2876–2887.
28. Kohno T, et al. Possible origin of adult T-cell leukemia/lymphoma cells from human T lymphotropic virus type-1-infected regulatory T cells. *Cancer Sci*. 2005;96(8):527–533.
29. Satou Y, Utsunomiya A, Tanabe J, Nakagawa M, Nosaka K, Matsuoka M. HTLV-1 modulates the frequency and phenotype of FoxP3+CD4+ T cells in virus-infected individuals. *Retrovirology*. 2012;9:46.
30. Toulza F, et al. Human T-lymphotropic virus type 1-induced CC chemokine ligand 22 maintains a high frequency of functional FoxP3+ regulatory T cells. *J Immunol*. 2010;185(1):183–189.
31. Hieshima K, Nagakubo D, Nakayama T, Shirakawa AK, Jin Z, Yoshie O. Tax-inducible production of CC chemokine ligand 22 by human T cell leukemia virus type 1 (HTLV-1)-infected T cells promotes preferential transmission of HTLV-1 to CCR4-expressing CD4+ T cells. *J Immunol*. 2008;180(2):931–939.
32. Grant C, Oh U, Yao K, Yamano Y, Jacobson S. Dysregulation of TGF-β signaling and regulatory and effector T-cell function in virus-induced neuroinflammatory disease. *Blood*. 2008;111(12):5601–5609.
33. Ohsugi T, Kumasaka T. Low CD4/CD8 T-cell ratio associated with inflammatory arthropathy in human T-cell leukemia virus type I Tax transgenic mice. *PLoS One*. 2011;6(4):e18518.
34. Iwakura Y, et al. Induction of inflammatory arthropathy resembling rheumatoid arthritis in mice transgenic for HTLV-I. *Science*. 1991;253(5023):1026–1028.
35. Nakamaru Y, et al. Immunological hyperresponsiveness in HTLV-I LTR-env-pX transgenic rats: a prototype animal model for collagen vascular and HTLV-I-related inflammatory diseases. *Pathobiology*. 2001;69(1):11–18.
36. Hanon E, et al. High production of interferon gamma but not interleukin-2 by human T-lymphotropic virus type I-infected peripheral blood mononuclear cells. *Blood*. 2001;98(3):721–726.
37. Yamazato Y, Miyazato A, Kawakami K, Yara S, Kaneshima H, Saito A. High expression of p40(tax) and pro-inflammatory cytokines and chemokines in the lungs of human T-lymphotropic virus type 1-related bronchopulmonary disorders. *Chest*. 2003;124(6):2283–2292.
38. Nakamura N, et al. Human T-cell leukemia virus type 1 Tax protein induces the expression of STAT1 and STAT5 genes in T-cells. *Oncogene*. 1999;18(17):2667–2675.
39. Sun SC, Yamaoka S. Activation of NF-kappaB by HTLV-I and implications for cell transformation. *Oncogene*. 2005;24(39):5952–5964.
40. Lazarevic V, Glimcher LH. T-bet in disease. *Nat Immunol*. 2011;12(7):597–606.
41. Nishiura Y, Nakamura T, Fukushima N, Moriuchi R, Katamine S, Eguchi K. Increased mRNA expression of Th1-cytokine signaling molecules in patients with HTLV-I-associated myelopathy/tropical spastic paraparesis. *Tohoku J Exp Med*. 2004;204(4):289–298.
42. Trejo SR, Fahl WE, Ratner L. The tax protein of human T-cell leukemia virus type 1 mediates the transactivation of the c-sis/platelet-derived growth factor-B promoter through interactions with the zinc finger transcription factors Sp1 and NGFI-A/Egr-1. *J Biol Chem*. 1997;272(43):27411–27421.
43. Furuya T, et al. Heightened transmigrating activity of CD4-positive T cells through reconstituted basement membrane in patients with human T-lymphotropic virus type I-associated myelopathy. *Proc Assoc Am Physicians*. 1997; 109(3):228–236.
44. Moritoyo T, et al. Detection of human T-lymphotropic virus type I p40tax protein in cerebrospinal fluid cells from patients with human T-lymphotropic virus type I-associated myelopathy/tropical spastic paraparesis. *J Neurovirol*. 1999;5(3):241–248.
45. Umehara F, Izumo S, Ronquillo AT, Matsumuro K, Sato E, Osame M. Cytokine expression in the spinal cord lesions in HTLV-I-associated myelopathy. *J Neuropathol Exp Neurol*. 1994;53(1):72–77.
46. Matsuura E, Yamano Y, Jacobson S. Neuroimmunity of HTLV-I Infection. *J Neuroimmune Pharmacol*. 2010;5(3):310–325.
47. Nagai M, Yamano Y, Brennan MB, Mora CA, Jacobson S. Increased HTLV-I proviral load and preferential expansion of HTLV-I Tax-specific CD8+ T cells in cerebrospinal fluid from patients with HAM/TSP. *Ann Neurol*. 2001;50(6):807–812.
48. Sato T, et al. CSF CXCL10, CXCL9, and neopterin as candidate prognostic biomarkers for HTLV-1-associated myelopathy/tropical spastic paraparesis. *PLoS Negl Trop Dis*. 2013;7(10):e2479.
49. Yamamoto K, et al. Phase I study of KW-0761, a defucosylated humanized anti-CCR4 antibody, in relapsed patients with adult T-cell leukemia-lymphoma and peripheral T-cell lymphoma.

J Clin Oncol. 2010;28(9):1591–1598.
50. Ishida T, et al. Defucosylated anti-CCR4 monoclonal antibody (KW-0761) for relapsed adult T-cell leukemia-lymphoma: a multicenter phase II study. *J Clin Oncol.* 2012;30(8):837–842.
51. Yamano Y, Sato T. Clinical pathophysiology of human T-lymphotropic virus-type 1-associated myelopathy/tropical spastic paraparesis. *Front Microbiol.* 2012;3:389.
52. Yamamoto-Taguchi N, et al. HTLV-1 bZIP factor induces inflammation through labile Foxp3 expression. *PLoS Pathog.* 2013;9(9):e1003630.
53. Shimoyama M. Diagnostic criteria and classification of clinical subtypes of adult T-cell leukaemia-lymphoma. A report from the Lymphoma Study Group (1984–1987). *Br J Haematol.* 1991;79(3):428–437.
54. Osame M. Review of WHO Kagoshima meeting and diagnostic guidelines for HAM/TSP. In: Blattner W, ed. *Human Retrovirology: HTLV.* New York, New York, USA: Raven Press; 1990:191–197.
55. Tanaka Y, et al. An antigenic structure of the trans-activator protein encoded by human T-cell leukemia virus type-I (HTLV-I), as defined by a panel of monoclonal antibodies. *AIDS Res Hum Retroviruses.* 1992;8(2):227–235.
56. Yoshiki T, et al. Models of HTLV-I-induced diseases. Infectious transmission of HTLV-I in inbred rats and HTVL-I env-pX transgenic rats. *Leukemia.* 1997;11(suppl 3):245–246.
57. Kamihira S, et al. Intra- and inter-laboratory variability in human T-cell leukemia virus type-1 proviral load quantification using real-time polymerase chain reaction assays: a multi-center study. *Cancer Sci.* 2010;101(11):2361–2367.
58. Bai Y, et al. Effective transduction and stable transgene expression in human blood cells by a third-generation lentiviral vector. *Gene Ther.* 2003;10(17):1446–1457.
59. Nagata K, Ohtani K, Nakamura M, Sugamura K. Activation of endogenous c-fos proto-oncogene expression by human T-cell leukemia virus type I-encoded p40tax protein in the human T-cell line, Jurkat. *J Virol.* 1989;63(8):3220–3226.
60. Dull T, et al. A third-generation lentivirus vector with a conditional packaging system. *J Virol.* 1998;72(11):8463–8471.
61. Shin HJ, Lee JB, Park SH, Chang J, Lee CW. T-bet expression is regulated by EGR1-mediated signaling in activated T cells. *Clin Immunol.* 2009;131(3):385–394.

Human Pathology (2014) 45, 1192–1198

ELSEVIER

Human PATHOLOGY

www.elsevier.com/locate/humpath

Original contribution

Prognostic impact of microRNA-145 down-regulation in adult T-cell leukemia/lymphoma☆,☆☆

Hongjing Xia MD, PhD[a,1], Seiji Yamada MD, PhD[a,1], Mineyoshi Aoyama MD, PhD[b,1], Fumihiko Sato DMD, PhD[a], Ayako Masaki MD, PhD[a], Yan Ge MD[a], Masaki Ri MD, PhD[c], Takashi Ishida MD, PhD[c], Ryuzo Ueda MD, PhD[c,d], Atae Utsunomiya MD, PhD[e], Kiyofumi Asai MD, PhD[b], Hiroshi Inagaki MD, PhD[a,*]

[a]*Department of Anatomic Pathology and Molecular Diagnostics, Nagoya City University Graduate School of Medical Sciences, Nagoya 467-8601, Japan*
[b]*Department of Molecular Neurobiology, Nagoya City University Graduate School of Medical Sciences, Nagoya 467-8601, Japan*
[c]*Department of Medical Oncology and Immunology, Nagoya City University Graduate School of Medical Sciences, Nagoya 467-8601, Japan*
[d]*Department of Tumor Immunology, Aichi Medical University School of Medicine, Nagakute 480-1195, Japan*
[e]*Department of Hematology, Imamura Bun-in Hospital, Kagoshima 890-0064, Japan*

Received 17 October 2013; revised 16 January 2014; accepted 24 January 2014

Keywords:
Adult T-cell leukemia/lymphoma;
Prognosis;
MicroRNAs;
Array analysis;
miR-145

Summary Adult T-cell leukemia/lymphoma (ATL) is a highly aggressive tumor caused by human T-cell leukemia virus type 1. MicroRNAs (miRNAs) are closely involved in the development and progression of various tumors. Here we investigated the dysregulation of miRNAs in ATL and its clinical significance. Studies using miRNA arrays and subsequent real-time reverse transcription polymerase chain reaction showed that, in the 9 ATL cell lines examined, 1 miRNA was consistently up-regulated, whereas another 3 were consistently down-regulated, compared with normal CD4-positive lymphocytes. Next, we analyzed the prognostic impact of these 4 miRNAs in patients with aggressive-type ATL (n = 40). Of the 4 dysregulated miRNAs selected, 3 (miR-130b higher expression, miR-145 lower expression, and miR-223 lower expression) were significantly associated with a worsened overall patient survival. We found that expressions of these 3 miRNAs were correlated with each other. To clarify which of the 3 had the most significant impact on overall survival, we performed a multivariate prognostic analysis that included these 3 miRNAs, and only miR-145 lower expression was selected as an independent risk factor ($P = .0005$). When overexpressed in an ATL cell line in vitro, miR-145 specifically inhibited tumor cell growth. In conclusion, our study suggests that miR-145 down-regulation provides a growth advantage in ATL and is highly associated with a worsened prognosis for patients with ALT. Hence, miR-145 may be a useful prognostic marker and a potential therapeutic target for ATL.

☆ Funding/Support: This study was supported in part by a Grant-in-Aid for Scientific Research from the Ministry of Education, Culture, Sports, Science, and Technology (MEXT), Japan, and by a Grant-in-Aid from the Ministry of Health, Labor, and Welfare.
☆☆ Competing interests: None.
* Corresponding author.
E-mail address: hinagaki@med.nagoya-cu.ac.jp (H. Inagaki).
[1] These authors contributed equally to this work.

http://dx.doi.org/10.1016/j.humpath.2014.01.017
0046-8177/

1. Introduction

MicroRNAs (miRNAs) are 18- to 25-nucleotide, single-stranded noncoding RNA molecules that play an important regulatory role by targeting mRNAs for repressing translation or mRNA cleavage [1]. They are transcribed with primary miRNAs, transported into the cytoplasm, cleaved into mature miRNAs, and then loaded onto the miRNA-induced silencing complex for RNA interference. The miRNA-induced silencing complex is guided to its mRNA target by the miRNA strand, which typically base pairs imperfectly to its target in the 3′ untranslated region, signaling the target for translational repression or degradation. Global changes of miRNAs are closely involved in neoplastic processes and tumor progression, and differential expression of miRNAs has been described in various tumors [2,3].

Human T-cell leukemia virus type 1 (HTLV-1) is a retrovirus known to be an etiologic agent of adult T-cell leukemia/lymphoma (ATL) [4]. More than 20 million people are infected with HTLV-1 worldwide, with the highest prevalence in southwest Japan and the Caribbean basin. HTLV-1 infection has a long clinical latency before transforming into ATL. It has a very poor prognosis because tumor cells are usually resistant to conventional chemotherapeutic agents [5,6]. Patients with ATL are typically highly immunocompromised and have frequent severe infections. Tumor cells from most patients with ATL are positive for CD4, CD25, and FOXP3. These immunologic and phenotypic characteristics of ATL are similar to those of regulatory T cells, and it has been suggested that ATL cells may originate from regulatory T cells, which actively suppress activation of the immune system [7].

Recently, some miRNAs have been shown to be involved in ATL [8-13]. However, oncogenetic and clinical significance of miRNAs have not been well clarified. In this study, we examined ATL cell lines and clinical ATL cases for miRNA expression using miRNA arrays, quantitative reverse transcription (RT) polymerase chain reaction (PCR), and the miRNA transfection assay.

2. Materials and methods

2.1. ATL cell lines and normal CD4-positive T cells

The 9 cell lines used in this study were as follows; ATL-102, ATN-1, HUT-102, MJ, MT-1, MT-2, MT-4, TL-Om1, and TL-SU. These cell lines were cultured in RPMI 1640 media supplemented with 10% fetal bovine serum, 50 U/mL penicillin, and 50 μg/mL streptomycin (Invitrogen, GIBCO, Carlsbad, CA), at 37°C with 5% CO_2. Mononuclear cells obtained from healthy volunteers (n = 4) were sorted into CD4-positive T cells.

2.2. Patients with ATL

Forty specimens from patients with aggressive ATL of the acute- or lymphoma-type [5] were retrieved from the pathology files of Nagoya City University, Graduate School of Medical Sciences, and Imamura Bun-in Hospital. All specimens were obtained at the initial presentation of the patients and were fixed in formalin and embedded in paraffin. All cases were positive for monoclonal integration of HTLV-1 provirus DNA. The pathological specimens were reviewed according to criteria of the World Health Organization classification of malignant lymphomas [6]. The median age at diagnosis was 60 years (range, 42-88 years), with a male-to-female ratio of approximately 1:1. All cases were within the morphologic boundaries of ATL and exhibited the following immunophenotypes: CD20−, CD3+, CD5+, CD4+, and CD25+. Thirty-three cases were histologically classified as the pleomorphic medium-large cell type, 3 as the pleomorphic small cell type, 3 as the anaplastic type, and 1 as the Hodgkin-like type. All patients were treated with doxorubicin-containing combination chemotherapy regimens. The study was approved by the institutional review board of Nagoya City University.

2.3. miRNA expression array

Using a flash PAGE system (Ambion, Carlsbad, CA), miRNA was extracted from 4 ATL cell lines (ATN-1, HUT-102, MJ, and TL-Om1). For the miRNA microarray, CD4-positive T-cell samples obtained from peripheral blood of 4 healthy volunteers were evenly mixed, and miRNA was extracted and used as a control miRNA. ATL has been suggested to originate from regulatory T cells, which are less than 2% of total CD4-positive cells in peripheral blood [14] and include 2 subsets, naturally occurring and inducible types [15]. Because it was difficult to obtain sufficient numbers of regulatory T cells for the experiment and to induce regulatory T cells specifically, we used CD4-positive T cells as a control in this study. miRNA samples were labeled with Cy-5 using a Label IT miRNA Labeling kit (Mirus Bio, Madison, WI) and hybridized to the array slides (mirVana miRNA Bioarray V2; Ambion). Signals were scanned with an Axon GenePix 4000B scanner (Molecular Devices, Sunnyvale, CA), and the miRNA array data thus obtained were analyzed using a Microarray Data Analysis Tool (Filgen, Nagoya, Japan) to select miRNAs significantly up- or down-regulated in all 4 ATL lines compared with control normal CD4-positive T cells.

2.4. miRNA isolation and quantitative RT-PCR in ATL cell lines

Total RNA extracted from fresh ATL cell lines (n = 9) and normal CD4-positive T cells from the 4 healthy volunteers was further miRNA-enriched using a PureLink miRNA

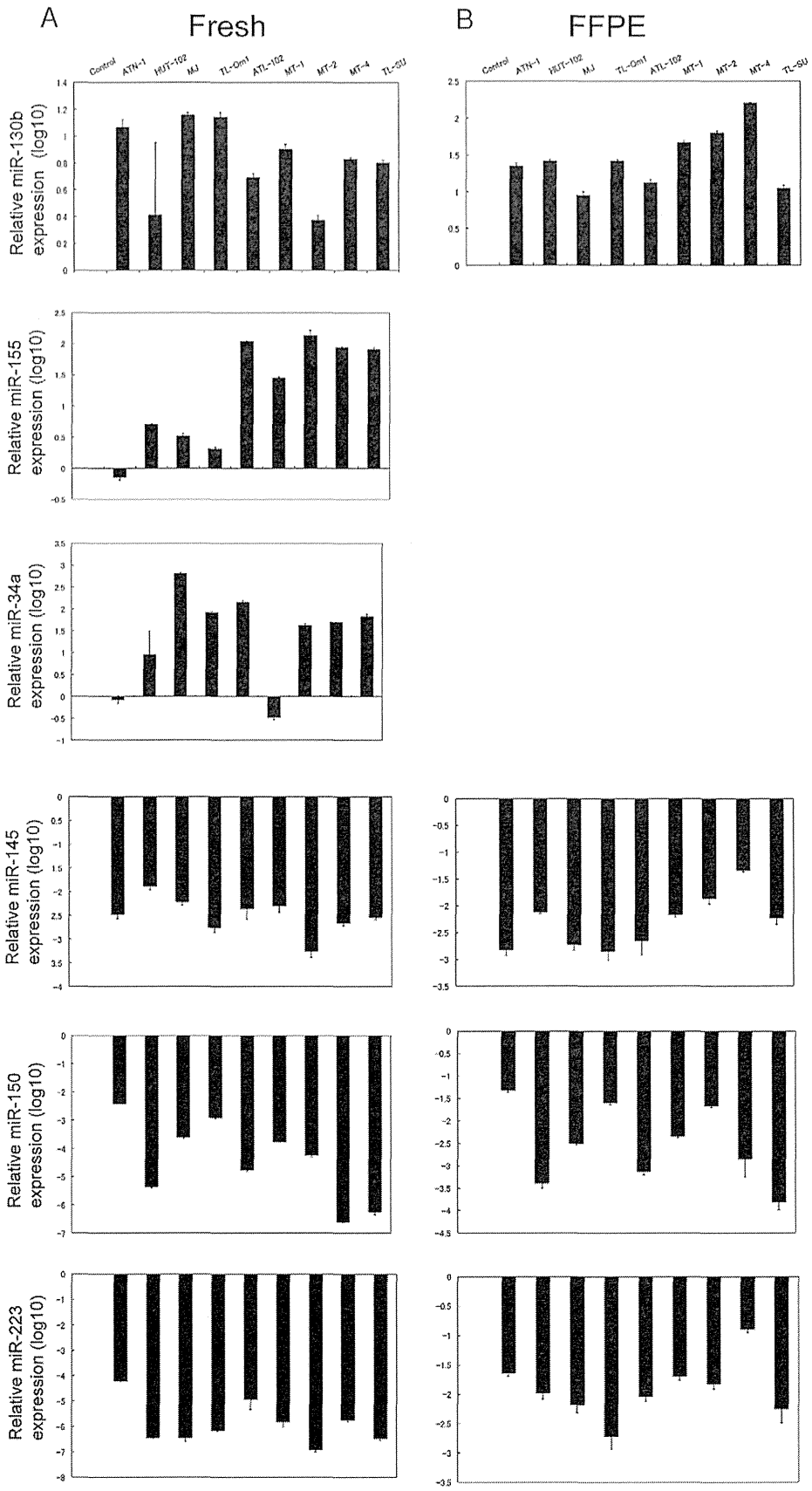

Fig. 1 Relative expression (log 10) of 6 miRNAs (miR-130b, miR-155, miR-34a, miR-145, miR-150, and miR-223) in 9 ATL cell lines (ATN-1, HUT102, MJ, TL-Om1, ATL-102, MT-1, MT-2, MT-4, and TL-SU). The 6 graphs (A) show levels using fresh ATL cell lines, and the 4 graphs (B) show levels using formalin-fixed, paraffin-embedded (FFPE) ATL cell lines.

Isolation kit (Invitrogen, Tokyo, Japan). Quantitative RT-PCR for the targeted mature miRNAs was performed using TaqMan MicroRNA Reverse Transcription kit (Applied Biosystems, Foster City, CA) and a TaqMan MicroRNA Assay kit (Applied Biosystems). All PCR reactions were run in triplicate, and miRNA expression relative to control RNU6B was calculated using the $2^{-\Delta\Delta Ct}$ method. The expression of miRNAs in T cells from the 4 healthy individuals was used as a quantitative control. ATL cell lines were fixed in formalin and embedded in paraffin. miRNAs extracted from the paraffin sections were subjected to quantitative RT-PCR to confirm that the target miRNAs were correctly quantified using paraffin sections as well.

2.5. miRNA expression in patients with ATL

Enriched total miRNA was extracted from paraffin-embedded materials of CD4-positive T cells from healthy patients and patients with ATL. Expression of target miRNAs was similarly semiquantified using quantitative RT-PCR. Cutoff values for higher or lower expression of respective miRNAs were set to give superior segregation into prognostic groups in overall survival. For patients with ATL, selected miRNAs were correlated with various clinicopathological factors (age, sex, the presence of B symptoms, extranodal sites, bone marrow involvement, serum lactate dehydrogenase (LDH) values more than twice the normal upper limit [5], histologic lymphoma subtype, and overall survival of the patients).

2.6. miRNA transfection and cell viability and death

MT-4 ATL cells (2×10^6) were resuspended in 100 μL of Nucleofector solution (Cell Line Nucleofector Kit V; Amaxa Biosystems, Cologne, Germany). Cells were electroporated with 100 and 300 nmol/L pre-miR has-miR-145 miRNA precursor, and a pre-miR negative control no. 1 using a Nucleofector (Pre-miR miRNA precursor Starter Kit; Ambion). Transfected cells were plated onto 6-well plates, and 1 mL/well antibiotic-free medium was added for incubation at 37°C with 5% CO_2. After 6 hours, 1.5 mL/well RPMI 1640 media supplemented with 10% fetal bovine serum, 50 U/mL penicillin, and 50 μg/mL streptomycin were added. Cells were plated in 96-well plates at 6×10^3 cells/well and cultured for 0, 24, 48, and 72 hours to test their viability using a methyl thiazolyl tetrazorium (MTT). The remaining cells were extracted for miRNA using an miRNA Isolation kit (Invitrogen) to verify electroporation quality.

2.7. Statistical analysis

All statistical analyses were performed using JMP (SAS, Cary, NC). The relationship between miRNA expression and various clinicopathological factors was evaluated using the Mann-Whitney U test or Fisher exact test. Survival curves were plotted using the Kaplan-Meier method, and the Cox proportional hazards model was applied for univariate and multivariate prognostic analysis. The in vitro data were analyzed using a paired t test. A probability value of $P < .05$ was regarded as statistically significant. All tests were 2 tailed.

3. Results

3.1. miRNA array analysis using ATL cell lines

Using miRNA array analysis, we profiled 4 ATL cell lines (ATN-1, HUT-102, MJ, and TL-Om1) using normal CD4-positive T cells as a control. In these 4 ATL cell lines, 3 miRNAs (miR-34a, miR-130b, and miR-155) were consistently highly up-regulated, and 3 miRNAs (miR-145, miR-150, and miR-223) were consistently highly down-regulated (Supplementary Fig. S1). To confirm the results of miRNA array data, we quantified these 6 miRNAs using quantitative real-time RT-PCR with the fresh 9 ATL cell lines (ATN-1, HUT-102, MJ, TL-Om1, ATL-102, MT-1, MT-2, MT-4, and TL-SU), including the 4 ATL cell lines used for miRNA array analysis (Fig. 1A). Of the 6 miRNAs tested, 4 (miR-130b, miR-145, miR-223, and miR-150) were consistently up- or down-regulated in the 9 ATL cell lines (Fig. 1A). Although up-regulated in the miRNA array, miR-34a and miR-155 were down-regulated in 1 and 2 of the 9 ATL cell lines, respectively (Fig. 1A), and we excluded these 2 miRNAs. The remaining 4 miRNAs were precisely quantified by quantitative RT-PCR using formalin-fixed, paraffin-embedded ATL cell lines as well (Fig. 1B).

Table Univariate and multivariate prognostic analyses of miRNAs for overall survival of the patients with ATL

miRNA	Expression	Overall survival					
		Univariate			Multivariate		
		P	Hazard ratio	95% CI	*P*	Hazard ratio	95% CI
miR130b	Higher	.0017	1.83	1.24-2.83	NS		
miR145	Lower	<.0001	3.01	1.79-5.16	.0005	2.59	1.52-4.49
miR150	Lower	NS					
miR223	Lower	.0010	0.96	1.29-3.25	NS		

Abbreviations: CI, confidence interval; NS, not significant.

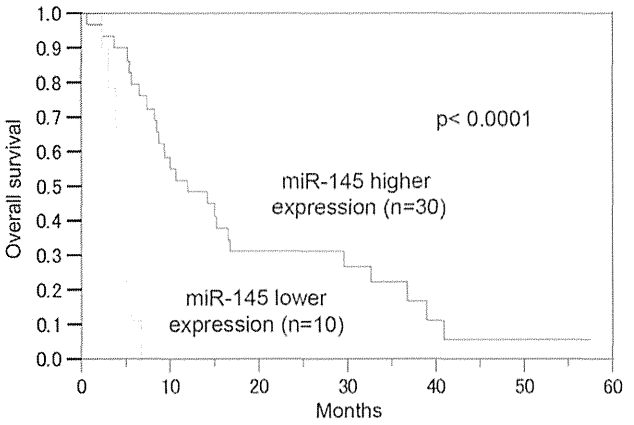

Fig. 2 Overall survival analysis of patients with ATL for miR-145 expression.

3.2. Expression of miRNAs in clinical ATL samples

Using quantitative RT-PCR, 40 clinical ATL cases (paraffin-embedded tumor samples) were examined for expression levels of the selected 4 miRNAs (miR-130b, miR-145, miR-150, and miR-223). To explore miRNAs highly associated with the clinical course, the prognostic impact of the 4 miRNAs on the overall survival of patients with ATL was analyzed. As shown in the Table, using a respective cutoff value that showed superior segregation into prognostic groups, 28 cases were higher expressers for miR-130b ($P = .0017$) and 10 cases each were lower expressers for miR-145 ($P < .0001$) and miR-223 ($P = .0010$). Expression of miR-150 failed to show any prognostic impact. The 3 miRNAs that showed a prognostic impact

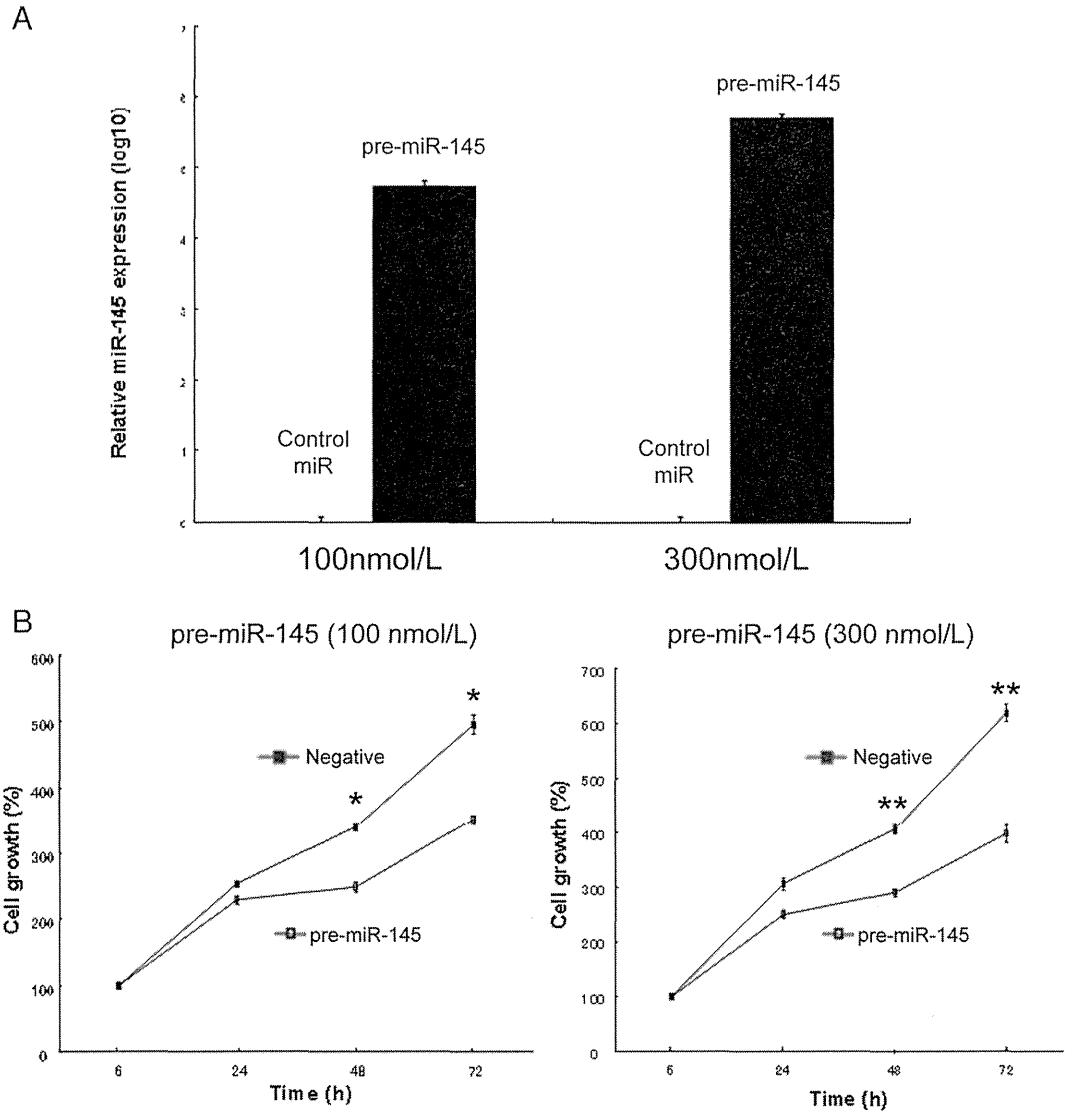

Fig. 3 miR-145 transfection assay. A, Relative expression (log 10) of miR-145 in ATL cells (MT-4) transfected with pre–miR-145 precursor or with negative control pre-miRNA precursor after a 48-hour incubation at a final concentration of 100 (left) or 300 nM (right). B, The effect of pre–miR-145 on growth of ATL cells (MT-4) as determined by an MTT assay. Cell proliferation is significantly inhibited by enforced expression of miR-145. The data represent the means ± SEM of 4 independent experiments. $*P < .05$ and $**P < .01$.

were found to be associated with each other (miR-130b versus miR-145, $P = .019$; miR-130b versus miR-223, $P < .0001$; and miR-145 versus miR-223, $P = .043$). To explore which miRNA was the most associated with the patients' prognosis, we performed a multivariate analysis. Only miR-145 lower expression was selected as a prognostic factor ($P = .0005$; hazard ratio, 2.59 [1.52-4.49]), whereas the other 2 miRNAs failed to achieve statistical significance (Table). Fig. 2 shows the overall survival curve of patients with ATL for miR-145 expression. miR-145 expression of patients with ATL relative to that of normal CD4-positive T cells was 0.0495 ± 0.0276 and 3.02 ± 1.03 (mean ± SEM) for lower and higher expressers, respectively. When correlated with clinicopathological factors including age, sex, the presence of B symptoms, performance status, extranodal sites, bone marrow involvement, elevated LDH value, and histologic lymphoma subtype, miR-145 lower expression was not associated with any of these factors.

3.3. Overexpression of miR-145 and cell growth inhibition in ATL cells

Because miR-145 was consistently down-regulated in ATL cell lines and showed the highest prognostic impact on patients' survival, we focused on this miRNA in further analysis. To examine the association between miR-145 expression and the growth of ATL cells, MT-4 cells were transfected with a pre–miR-145 precursor and a pre-miR negative control, and an MTT assay was conducted. Overexpression of mature miR-145 in the transfected cells was confirmed by quantitative RT-PCR (Fig. 3A). Cell growth was significantly inhibited in cells transfected with pre–miR-145 48 hours after the transfection by approximately 40% as compared with those transfected with the pre-miR negative control (Fig. 3B). These results indicated that miR-145 specifically inhibited the cell growth of the MT-4 cell line.

4. Discussion

In this study, we found that 1 miRNA (miR-130b) was consistently up-regulated, and 3 (miR-145, miR-223, and miR-150) were consistently down-regulated in ATL cell lines using an miRNA array and subsequent quantitative RT-PCR. It has been shown that expression of some of these miRNAs is dysregulated in ATL cell lines: miR-130b and miR223 have been reported to be up-regulated [8] and down-regulated [10], respectively. miR155, which was selected in the present miRNA array but was subsequently excluded because of its inconsistent expression in the quantitative RT-PCR, has been frequently up-regulated in ATL [9,10,13]. It is difficult to explain this discrepancy. A similar observation was reported in cutaneous T-cell lymphoma, and it was speculated that cross-hybridization of pre–miR-155 to the hybridization probe might have masked the signal of the mature miR-155 [16]. Recently, Yamagishi et al [11] and Tomita et al [12] determined the miRNA signatures and revealed miR-31 down-regulation and miR-146a up-regulation in primary ATL cells, respectively. However, these 2 miRNAs were not highly dysregulated in our miRNA array. This is partly explained by our use of the ATL tumor samples and control samples. For the ATL tumor samples and controls, we used ATL cell lines and normal CD4-positive lymphocytes while Yamagishi et al used clinical ATL cells as tumor samples [11] and Tomita et al used HTLV-1–uninfected T-cell lines as a control [12].

Of the 4 dysregulated miRNAs we determined (miR-130b, miR-145, miR-150, and miR-223), we searched for miRNAs that had a prognostic impact on clinical ATL cases. For each of the 4 miRNAs, we divided our ATL cases into 2 groups (higher and lower expression) using a respective cutoff value that showed superior segregation into prognostic groups. Univariate prognostic analysis showed that miR-130b, miR-145, and miR-223, but not miR-150, had a significant association with the overall survival of patients with ATL. The reason why miR-150 did not achieve statistical significance is difficult to discern, but may be partly explained as follows. First, some miRNAs are expressed differently in ATL cell lines compared with clinical samples, and miR-150 was reported to be differentially expressed in ATL cell lines and uncultured ATL cells [9]. Second, miR-150 may be more associated with tumor development than tumor progression.

We found that the expressions of 3 selected miRNAs (miR-130b, miR-145, and miR-223) were significantly associated with each other. Multivariate prognostic analysis including these 3 miRNAs revealed that only miR-145 lower expression achieved statistical significance. Interestingly, this miRNA was not correlated with any of the clinicopathological or risk factors examined, suggesting that miR-145 lower expression might be a useful independent prognostic factor. Although down-regulated in all ATL cell lines examined, miR-145 was not always down-regulated in patients with clinical ATL. One possible explanation may be that ATL cell line tumor cells are highly activated and more aggressive than clinical ATL cases.

We then focused on miR-145, and to confirm whether miR-145 expression was inversely associated with ATL cell proliferation, we performed an MTT assay to measure cell proliferation rates before and after enforced miR-145 expression in an ATL cell line, MT-4, and showed that overexpression of miR-145 significantly inhibited tumor cell growth. This inhibition was not complete, suggesting that some other factors or pathways may be involved in tumor cell growth. Down-regulation of miR-145 has been reported in various types of human carcinoma [17-20] and B-cell malignancy [21-23]. These studies suggest that miR-145 plays a role in controlling cell proliferation, thereby serving as a tumor suppressor. The precise upstream mechanism of miR-145 down-regulation in ATL has not been clarified.

Recently, down-regulation of miR-145 by DNA methylation and p53 mutation pathways has been suggested in prostate cancer [24]. We searched a Web site (microRNA.org-Targets and Expression; http://microrna.org/microrna) for specific targets of miR-145 and retrieved more than 20 targets with high matching scores. However, no association has been suggested between these candidate targets and ATL in the literature. Potential targets of miR-145 have been reported including MYC in colon cancer [25], ERG in prostate cancer [26], and connective tissue growth factor in glioblastoma [27].

In conclusion, we investigated ATL cell lines and clinical ATL cases for miRNA expression using miRNA arrays and quantitative RT-PCR, and we found that down-regulation of miR-145 was highly associated with a worsened clinical course in patients. An in vitro functional assay showed that miR-145 expression was inversely associated with tumor cell proliferation. To the best of our knowledge, the involvement of miR-145 in ATL has not been reported. Our findings shed light on the biological and clinical roles of miR-145 in ATL and provide the basis for the development of new miRNA-targeted therapeutic strategies against this tumor.

Supplementary data

Supplementary data to this article can be found online at http://dx.doi.org/10.1016/j.humpath.2014.01.017.

Acknowledgments

We thank Mr T. Sakakibara and Dr H. Takino for their valuable comments.

References

[1] Bartel DP. MicroRNAs: genomics, biogenesis, mechanism, and function. Cell 2004;116:281-97.
[2] Kato M, Slack FJ. MicroRNAs: small molecules with big roles: *C. elegans* to human cancer. Biol Cell 2008;100:71-81.
[3] Kong YW, Ferland-McCollough D, Jackson TJ, Bushell M. microRNAs in cancer management. Lancet Oncol 2012;13:e249-58.
[4] Matsuoka M, Jeang KT. Human T-cell leukaemia virus type 1 (HTLV-1) infectivity and cellular transformation. Nat Rev Cancer 2007;7:270-80.
[5] Shimoyama M. Diagnostic criteria and classification of clinical subtypes of adult T-cell leukaemia-lymphoma: a report from the Lymphoma Study Group (1984-87). Br J Haematol 1991;79:428-37.
[6] Ohshima K, Jaffe ES, Kikuchi M. Adult T-cell leukemia/lymphoma. In: Swerdlow E, Campo NL, Harris ES, et al, editors. WHO classification of tumours of haematopoietic and lymphoid tissues. 4th ed. Lyon: IARC Press; 2008. p. 281-4.
[7] Ishida T, Ueda R. Immunopathogenesis of lymphoma: focus on CCR4. Cancer Sci 2011;102:44-50.
[8] Yeung ML, Yasunaga J, Bennasser Y, et al. Roles for microRNAs, miR-93 and miR-130b, and tumor protein 53-induced nuclear protein 1 tumor suppressor in cell growth dysregulation by human T-cell lymphotrophic virus 1. Cancer Res 2008;68:8976-85.
[9] Bellon M, Lepelletier Y, Hermine O, Nicot C. Deregulation of microRNA involved in hematopoiesis and the immune response in HTLV-1 adult T-cell leukemia. Blood 2009;113:4914-7.
[10] Pichler K, Schneider G, Grassmann R. MicroRNAs miR-146a and further oncogenesis-related cellular microRNAs are dysregulated in HTLV-1 transformed T lymphocytes. Retrovirology 2008;5:100.
[11] Yamagishi M, Nakano K, Miyake A, et al. Polycomb-mediated loss of miR-31 activates NIK-dependent NF-kB pathway in adult T cell leukemia and other cancers. Cancer Cell 2012;21:121-35.
[12] Tomita M, Tanaka Y, Mori N. MicroRNA miR-146a is induced by HTLV-1 Tax and increases the growth of HTLV-1 infected T-cells. Int J Cancer 2012;130:2300-9.
[13] Ishihara K, Sasaki D, Tsuruda K, et al. Impact of miR-155 and miR-126 as novel biomarkers on the assessment of disease progression and prognosis in adult T-cell leukemia. Cancer Epidemiol 2012;36:560-5.
[14] Baecher-Allan C, Brown JA, Freeman GJ, Hafler DA. CD4+CD25 high regulatory cells in human peripheral blood. J Immunol 2001;167:1245-53.
[15] Sakaguchi S, Miyara M, Costantino CM, Hafler DA. FOXP3+ regulatory T cells in the human immune system. Nat Rev Immunol 2010;10:490-500.
[16] Ralfkiaer U, Hagedorn RH, Bangsgaard N, et al. Diagnostic microRNA profiling in cutaneous T-cell lymphoma (CTCL). Blood 2011;118:5891-900.
[17] Sempere LF, Christensen M, Silahtaroglu A, et al. Altered microRNA expression confined to specific epithelial cell subpopulations in breast cancer. Cancer Res 2007;67:11612-20.
[18] Cho WC, Chow AS, Au JS. Restoration of tumour suppressor hsa-miR-145 inhibits cancer cell growth in lung adenocarcinoma patients with epidermal growth factor receptor mutation. Eur J Cancer 2009;45:2197-206.
[19] Zaman MS, Chen Y, Deng G, et al. The functional significance of microRNA-145 in prostate cancer. Bri J Cancer 2010;103:256-64.
[20] Gao P, Wong CC, Tung EK, Lee JM, Wong CM, Ng IO. Deregulation of microRNA expression occurs early and accumulates in early stages of HBV-associated multistep hepatocarcinogenesis. J Hepatol 2011;54:1177-84.
[21] Akao Y, Nakagawa Y, Kitada Y, Kinoshita T, Naoe T. Down-regulation of microRNAs-143 and -145 in B-cell malignancies. Cancer Sci 2007;98:1914-20.
[22] Roehle A, Hoefig KP, Repsilber D, et al. MicroRNA signatures characterize diffuse large B-cell lymphomas and follicular lymphomas. Br J Haematol 2008;142:732-44.
[23] Fischer L, Hummel M, Korfel A, Lenze D, Joehrens K, Thiel E. Differential micro-RNA expression in primary CNS and nodal diffuse large B-cell lymphomas. Neuro-Oncol 2011;13:1090-8.
[24] Suh SO, Chen Y, Zaman MS, et al. MicroRNA-145 is regulated by DNA methylation and p53 gene mutation in prostate cancer. Carcinogenesis 2011;32:772-8.
[25] Sachdeva M, Zhu S, Wu F, et al. p53 represses c-Myc through induction of the tumor suppressor miR-145. Proc Natl Acad Sci U S A 2009;106:3207-12.
[26] Hart M, Wach S, Nolte E, et al. The proto-oncogene ERG is a target of microRNA miR-145 in prostate cancer. FEBS J 2013;280:2105-16.
[27] Lee HK, Bier A, Cazacu S, et al. MicroRNA-145 is downregulated in glial tumors and regulates glioma cell migration by targeting connective tissue growth factor. PLoS One 2013;8:e54652.

Published OnlineFirst April 11, 2014; DOI: 10.1158/1078-0432.CCR-13-3169

Human Cancer Biology

Clinical Cancer Research

CADM1 Expression and Stepwise Downregulation of CD7 Are Closely Associated with Clonal Expansion of HTLV-I–Infected Cells in Adult T-cell Leukemia/Lymphoma

Seiichiro Kobayashi[1], Kazumi Nakano[5], Eri Watanabe[2], Tomohiro Ishigaki[2], Nobuhiro Ohno[3], Koichiro Yuji[3], Naoki Oyaizu[4], Satomi Asanuma[5], Makoto Yamagishi[5], Tadanori Yamochi[5], Nobukazu Watanabe[2], Arinobu Tojo[1,3], Toshiki Watanabe[5], and Kaoru Uchimaru[3]

Abstract

Purpose: Cell adhesion molecule 1 (CADM1), initially identified as a tumor suppressor gene, has recently been reported to be ectopically expressed in primary adult T-cell leukemia–lymphoma (ATL) cells. We incorporated CADM1 into flow-cytometric analysis to reveal oncogenic mechanisms in human T-cell lymphotrophic virus type I (HTLV-I) infection by purifying cells from the intermediate stages of ATL development.

Experimental Design: We isolated CADM1- and CD7-expressing peripheral blood mononuclear cells of asymptomatic carriers and ATLs using multicolor flow cytometry. Fluorescence-activated cell sorted (FACS) subpopulations were subjected to clonal expansion and gene expression analysis.

Results: HTLV-I–infected cells were efficiently enriched in $CADM1^{+}$ subpopulations (D, $CADM1^{pos}CD7^{dim}$ and N, $CADM1^{pos}CD7^{neg}$). Clonally expanding cells were detected exclusively in these subpopulations in asymptomatic carriers with high proviral load, suggesting that the appearance of D and N could be a surrogate marker of progression from asymptomatic carrier to early ATL. Further disease progression was accompanied by an increase in N with a reciprocal decrease in D, indicating clonal evolution from D to N. The gene expression profiles of D and N in asymptomatic carriers showed similarities to those of indolent ATLs, suggesting that these subpopulations represent premalignant cells. This is further supported by the molecular hallmarks of ATL, that is, drastic downregulation of miR-31 and upregulation of abnormal *Helios* transcripts.

Conclusion: The CADM1 versus CD7 plot accurately reflects disease progression in HTLV-I infection, and $CADM1^{+}$ cells with downregulated CD7 in asymptomatic carriers have common properties with those in indolent ATLs. *Clin Cancer Res; 20(11); 2851–61. ©2014 AACR.*

Introduction

Human T-cell lymphotrophic virus type I (HTLV-I) is a human retrovirus that causes HTLV-I–associated diseases, such as adult T-cell leukemia–lymphoma (ATL), HTLV-I–associated myelopathy/tropical spastic paraparesis, and HTLV-I uveitis (1–3). In Japan, the estimated lifetime risk of developing ATL in HTLV-I carriers is 6% to 7% for males and 2% to 3% for females (4–6). It takes several decades for HTLV-I–infected cells to reach the final stage of multistep oncogenesis, which is clinically recognized as aggressive ATL (acute-type and lymphoma-type; ref. 7). Molecular interaction of viral genes [e.g., Tax and the HTLV-I basic leucine zipper (HBZ) gene] with the cellular machinery causes various genetic and epigenetic alterations (7–11). However, difficulties in purifying HTLV-I–infected cells *in vivo* seem to have hindered understanding of the genetic events that are directly involved in the multistep oncogenesis of ATL.

Upregulation or aberrant expression of cell surface markers, such as CCR4 and CD25, is useful for diagnosis of ATL and has been utilized for molecular-targeted therapy (12, 13). However, the expression levels of these markers vary among patients, which often make it difficult to identify ATL cells specifically based on the immunophenotype. Previously, we focused on downregulated markers in acute-type ATL cells, such as CD3 and CD7, and successfully purified ATL cells using the CD3 versus CD7 plot of $CD4^{+}$ cells (14). Analysis of other clinical subtypes

Authors' affiliations: [1]Division of Molecular Therapy; [2]Laboratory of Diagnostic Medicine, Division of Stem Cell Therapy; [3]Department of Hematology/Oncology, Research Hospital; [4]Clinical Laboratory, Research Hospital, Institute of Medical Science; and [5]Graduate School of Frontier Sciences, The University of Tokyo, Tokyo, Japan

Note: Supplementary data for this article are available at Clinical Cancer Research Online (http://clincancerres.aacrjournals.org/).

Corresponding Author: Kaoru Uchimaru, Institute of Medical Science, The University of Tokyo, 4-6-1 Shirokanedai, Minato-ku, Tokyo 108-8639, Japan. Phone: 81-3-5449-5542; Fax: 81-3-5449-5429; E-mail: uchimaru@ims.u-tokyo.ac.jp

doi: 10.1158/1078-0432.CCR-13-3169

Published OnlineFirst April 11, 2014; DOI: 10.1158/1078-0432.CCR-13-3169

Translational Relevance

In this study, we showed that the cell adhesion molecule 1 (CAMD1) versus CD7 plot reflects the progression of disease in patients infected with human T-cell lymphotrophic virus type I (HTLV-I), in that the proportion of CADM1^{+} subpopulations (D, CADM1^{pos} CD7^{dim} and N, CADM1^{pos}CD7^{neg}) increased with the progression from HTLV-I asymptomatic carrier (AC) to indolent adult T-cell leukemia–lymphoma (ATL) to aggressive ATL. We confirmed the purity of the clonal HTLV-I–infected cells in these subpopulations of various clinical subtypes, including asymptomatic carriers. The results from the flow-cytometric analysis will help physicians assess disease status. The analysis is also practical in screening for putative high-risk HTLV-I asymptomatic carriers, which show nearly identical flow-cytometric and gene expression profiles with those of smoldering-type ATL patients. Furthermore, cell sorting by flow cytometry enables purification of clonally expanding cells in various stages of oncogenesis in the course of progression to aggressive ATL. Detailed molecular analysis of these cells will provide valuable information about the molecular events involved in multistep oncogenesis of ATL.

(indolent ATLs and HTLV-I asymptomatic carriers; AC) revealed that HTLV-I–infected and clonally expanded cells were purified similarly and that the subpopulations with downregulated CD7 grew concomitantly with the progression of HTLV-I infection (15). Although this type of flow-cytometric analysis was shown to be a useful tool, a substantial subpopulation of T cells shows downregulated expression of CD7 under physiologic (16, 17) and certain pathologic conditions, including autoimmune disorders, viral infection, and hematopoietic stem cell transplantation (18–23).

Recently, Sasaki and colleagues reported ectopic overexpression of the cell adhesion molecule 1/tumor suppressor in lung cancer 1 (CADM1/TSLC1) gene in primary acute-type ATL cells based on expression profile analysis (24, 25). CADM1 (/TSLC1) is a cell-adhesion molecule that was originally identified as a tumor suppressor in lung cancers (25, 26). In addition, numbers of CD4^{+} CADM1^{+} cells have been found to be significantly correlated with the proviral load (PVL) in both ATLs and HTLV-I asymptomatic carriers (25, 27). Thus, CADM1 is a good candidate marker of HTLV-I–infected cells. In the present study, we incorporated CADM1 into our flow-cytometric analysis. In the CADM1 versus CD7 plot of CD4^{+} cells, HTLV-I–infected and clonally expanded cells were efficiently enriched in the CADM1^{+} subpopulations regardless of disease status. In these cells, stepwise CD7 downregulation (from dimly positive to negative) occurred with disease progression. The proportion of the three subpopulations observed in this plot [P, CADM1$^{negative(neg)}$CD7$^{positive(pos)}$; D, CADM1^{pos}CD7^{dim}; and N, CADM1^{pos} CD7^{neg}] accurately reflected the disease status in HTLV-I infection. The analysis of comprehensive gene expression in each subpopulation revealed that the expression profile of CADM1^{+} subpopulations in indolent ATLs showed similarities with that in asymptomatic carriers with high PVL; yet, it was distinct from that in aggressive ATLs. These D and N subpopulations were indicative of HTLV-I–infected cells in the intermediate stage of ATL development.

Materials and Methods

Cell lines and patient samples

TL-Om1, an HTLV-I–infected cell line (28), was provided by Dr. Sugamura (Tohoku University, Sendai, Japan). The MT-2 cell line was a gift from Dr. Miyoshi (Kochi University, Kochi, Japan) and ST-1 was from Dr. Nagai (Nagasaki University, Nagasaki, Japan). Peripheral blood samples were collected from in-patients and out-patients at our hospital, as described in our previous reports (14, 15). As shown in Supplementary Table S1, 26 cases were analyzed (10 cases of asymptomatic carrier; 5 cases of smoldering-type; 6 cases of chronic-type; and 5 cases of acute-type). All patients with ATL were categorized into clinical subtypes according to Shimoyama's criteria (12, 29). Patients with various complications, such as autoimmune disorders and systemic infections, were excluded. Lymphoma-type patients were also excluded because ATL cells are not considered to exist in the peripheral blood of this clinical subtype. Samples collected from six healthy volunteers (mean age 48.8 years; range 34–66 years) were used as normal controls. The present study was approved by the Institutional Review Board of our institute (the University of Tokyo, Tokyo, Japan). Written informed consent was obtained from all patients and healthy volunteers.

Flow cytometry and cell sorting

Peripheral blood mononuclear cells (PBMC) were isolated from whole blood by density gradient centrifugation, as described previously (14). An unlabeled CADM1 antibody (clone 3E1) and an isotype control chicken immunoglobulin Y (IgY) antibody were purchased from MBL. These were biotinylated (primary amine biotinylation) using biotin N-hydroxysuccinimide ester (Sigma-Aldrich). Pacific Orange-conjugated anti-CD14 antibody was purchased from Caltag-Invitrogen. All other antibodies were obtained from BioLegend. Cells were stained using a combination of biotin-CADM1, allophycocyanin (APC)-CD7, APC-Cy7-CD3, Pacific Blue-CD4, and Pacific Orange-CD14. After washing, phycoerythrin-conjugated streptavidin was applied. Propidium iodide (Sigma-Aldrich) was added to the samples to stain dead cells immediately before flow cytometry. A FACSAria instrument (BD Immunocytometry Systems) was used for all multicolor flow cytometry and fluorescence-activated cell sorting (FACS). Data were analyzed using FlowJo software (TreeStar). The gating

Published OnlineFirst April 11, 2014; DOI: 10.1158/1078-0432.CCR-13-3169

procedure for a representative case is shown in Supplementary Fig. S1.

Quantification of HTLV-I proviral load by real-time quantitative PCR

PVL in FACS-sorted PBMCs was quantified by real-time quantitative PCR (TaqMan method) using the ABI Prism 7000 sequence detection system (Applied Biosystems), as described previously (14, 30).

Evaluation of HTLV-I *HBZ* gene amplification by semiquantitative PCR

HTLV-I *HBZ* gene amplification was performed as described previously (25). Briefly, the 25-μL PCR mixture consisted of 20 pmol of each primer, 2.0 μL of mixed deoxynucleotide triphosphates (2.5 mmol/L each), 2.5 μL of 10× PCR buffer, 1.5 μL of $MgCl_2$ (25 mmol/L), 0.1 μL of AmpliTaq Gold DNA Polymerase (Applied Biosystems), and 20 ng of DNA extracted from cell lines and clinical samples. The PCR consisted of initial denaturation at 94°C for 9 minutes, 30 cycles of 94°C for 30 seconds, 57°C for 30 seconds, and 72°C for 45 seconds, followed by 72°C for 5 minutes. The β-actin gene (*ACTB*) was used as an internal reference control. The primer sequences used were as follows: HBZ forward, 5′-CGCTGCCGATCACGATG-3′; HBZ reverse, 5′-GGAGGAATTGGTGGACG-3′; ACTB forward, 5′-CGTGCTCAGGGCTTCTT-3′; and ACTB reverse, 5′-TGAAGGTCTCAAACATGATCTG-3′. Amplification with these pairs of oligonucleotides yielded 177-bp HBZ and 731-bp β-actin fragments.

FISH for quantification of HTLV-I–infected cells

FISH analysis was performed to detect HTLV-I proviral DNA in mononuclear cells that had been FACS-sorted on the basis of the CADM1 versus CD7 plot. These samples were sent to a commercial laboratory (Chromosome Science Labo Inc.), where FISH analysis was performed. Briefly, pUC/HTLV-I plasmid containing the whole-HTLV-I genome was labeled with digoxigenin by the nick translation method, and was then used as a FISH probe. Pretreatment, hybridization, and washing were performed according to standard laboratory protocols. To remove fluorochrome-labeled antibodies attached to the cell surface, pretreatment consisted of treatment with 0.005% pepsin and 0.1 N HCl. The FISH probe was detected with Cy3-labeled anti-digoxigenin antibody. Cells were counterstained with 4′, 6 diamidino-2-phenylindole. The results were visualized using a DMRA2 conventional fluorescence microscope (Leica) and photographed using a Leica CW4000 cytogenetics workstation. Hybridization signals were evaluated in approximately 100 nuclei.

Inverse long PCR to assess the clonality of HTLV-I–infected cells

For clonality analysis, inverse long PCR was performed as described previously (14). First, 1 μg genomic DNA extracted from the FACS-sorted cells was digested with *PstI* or *Eco*RI at 37°C overnight. RNase A (Qiagen) was added to remove residual RNA completely. DNA fragments were purified using a QIAEX2 Gel Extraction Kit (Qiagen). The purified DNA was self-ligated with T4 DNA ligase (Takara Bio) at 16°C overnight. After ligation of the *Eco*RI-digested samples, the ligated DNA was further digested with *MluI*, which cuts the pX region of the HTLV-I genome and prevents amplification of the viral genome. Inverse long PCR was performed using Tks Gflex DNA Polymerase (Takara Bio). For the *PstI*-treated group, the forward primer was 5′-CAGCCCATTCTATAGCACTCTCCAGGAGAG-3′ and the reverse primer was 5′-CAGTCTCCAAACACGTAGACTGGGTATCCG-3′. For the *Eco*RI-treated template, the forward primer was 5′-TGCCTGACCCTGCTTGCTCAACTCTACGTCTTTG-3′ and the reverse primer was 5′-AGTCTGGGCCCTGACCTTTTCAGACTTCTGTTTC-3′. Processed genomic DNA (50 ng) was used as a template. The reaction mixture was subjected to 35 cycles of denaturation (94°C, 30 seconds) and annealing plus extension (68°C, 8 minutes). Following PCR, the products were subjected to electrophoresis on 0.8% agarose gels. Fourteen patient samples were analyzed. For samples from which a sufficient amount of DNA was extracted, PCR was generally performed in duplicate.

Gene expression microarray analysis of each subpopulation in the CADM1 versus CD7 plot

Total RNA was extracted from each subpopulation in the CADM1 versus CD7 plot using TRIzol (Invitrogen) according to the manufacturer's protocol. Details of the clinical samples used for microarray analyses are shown in Supplementary Table S1. Treatment with DNase I (Takara Bio) was conducted to eliminate genomic DNA contamination. The quality of the extracted RNA was assessed using a BioAnalyzer 2000 system (Agilent Technologies). The RNA was then Cy3-labeled using a Low Input Quick Amp Labeling Kit (Agilent Technologies). Labeled cRNA samples were hybridized to 44K Whole Human Genome Oligonucleotide Microarrays (Agilent Technologies) at 65°C for 17 hours. After hybridization, the microarrays were washed and scanned with a Scanner C (Agilent Technologies). Signal intensities were evaluated by Feature Extraction 10.7 software and then analyzed using Gene Spring 12.0 software (Agilent Technologies). Unsupervised two-dimensional hierarchical clustering analysis (Pearson correlation) was performed on 10,278 genes selected by one-way ANOVA ($P < 0.05$). The dataset for these DNA microarrays has been deposited in Gene Expression Omnibus (accession number GSE55851).

Expression analysis of miR-31 and *Helios* transcript variants of each subpopulation in the CADM1 versus CD7 plot

The expression levels of the microRNA miR-31 were quantified using a TaqMan-based MicroRNA Assay (Applied Biosystems), as described previously (31), and normalized to RNU48 expression level. Helios mRNA transcript variants were examined using reverse transcription

Published OnlineFirst April 11, 2014; DOI: 10.1158/1078-0432.CCR-13-3169

PCR (RT-PCR) with Platinum Taq DNA Polymerase High Fidelity (Invitrogen), as described previously (32). To detect and distinguish alternative splicing variants, PCR analyses were performed with sense and antisense primer sets specific for the first and final exons of the Helios gene. The PCR products were then sequenced to determine the exact type of transcript variant. A mixture of Hel-1, Hel-2, Hel-5, and Hel-6 cDNA fragments was used as a "Helios standard" in the electrophoresis of RT-PCR samples.

Results

CADM1 expression based on the CD3 versus CD7 plot in CD4$^+$ cells in primary HTLV-I–infected blood samples

The clinical profiles of the 32 cases analyzed are shown in Supplementary Table S1. We first examined CADM1 expression in each subpopulation (H, I, and L) of the CD3 versus CD7 plot. Representative data (for a case of smoldering ATL) are shown in Fig. 1A. The results demonstrate that

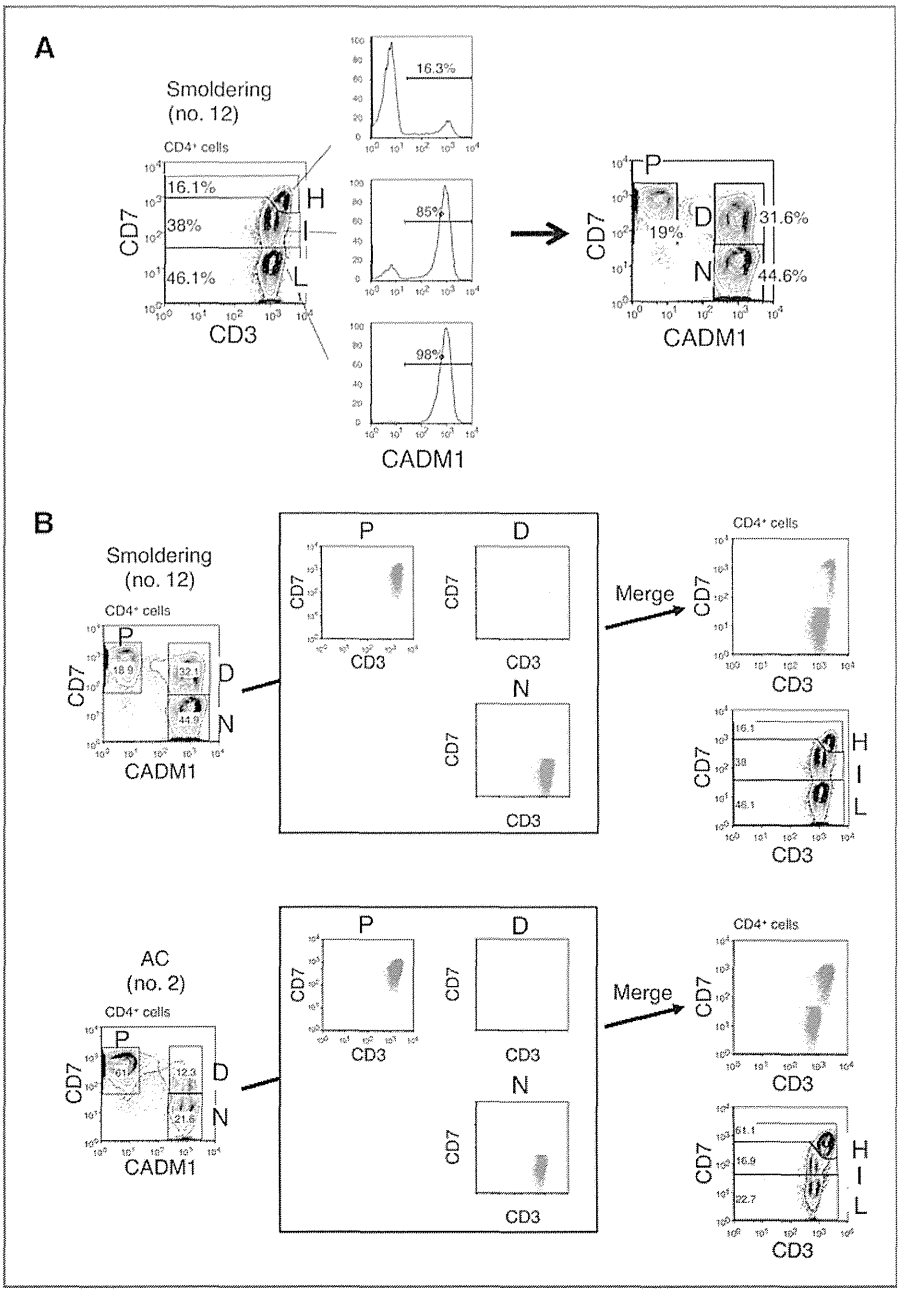

Figure 1. CADM1 versus CD7 plot for CD4$^+$ cells from HTLV-I–infected blood samples analyzed by flow cytometry. A, representative flow-cytometric analysis of a patient with smoldering-type ATL. Three subpopulations (H, I, and L) were observed in the CD3 versus CD7 plot for CD4$^+$ cells (left). Expression of CADM1 in each subpopulation is shown (middle). The right-hand panel shows how the CADM1 versus CD7 plot for CD4$^+$ cells was constructed. B, the P, D, and N subpopulations in the CADM1 versus CD7 plot correspond to the H, I, and L subpopulations in the CD3 versus CD7 plot. Blue, yellow, and red dots, respectively, indicate the P, D, and N subpopulations in the CADM1 versus CD7 plot, and are redrawn in the CD3 versus CD7 plot. Two representative cases are shown. In the upper case, the P and D subpopulations in the CADM1 versus CD7 plot are partly intermingled in the CD3 versus CD7 plot. Unlike the CD3 versus CD7 plot, the CADM1 versus CD7 plot clearly distinguishes three subpopulations.

Published OnlineFirst April 11, 2014; DOI: 10.1158/1078-0432.CCR-13-3169

CADM1 was expressed almost exclusively in the I and L subpopulations. Drawing a CADM1 versus CD7 plot for $CD4^+$ cells revealed three distinct subpopulations (P, $CADM1^{neg}CD7^{pos}$; D, $CADM1^{pos}CD7^{dim}$; and N, $CADM1^{pos}$ $CD7^{neg}$). As shown in Fig. 1B, the P, D, and N subpopulations corresponded to the H, I, and L subpopulations in the CD3 versus CD7 plot. In the previous CD3 versus CD7 plot, the lower case (AC no. 2) showed three distinct subpopulations. However, in the upper case (smoldering no. 12), the H and I subpopulations substantially intermingled with each other and were not clearly separated. In contrast, the CADM1 versus CD7 plot clearly revealed three distinct subpopulations in both cases.

HTLV-I–infected cells are highly enriched in $CADM1^+$ subpopulations

On the basis of previous reports (25, 27), we expected HTLV-I–infected cells to be enriched in the $CADM1^+$ subpopulations in our analysis. Figure 2A shows the PVL measurements of the three subpopulations in the CADM1 versus CD7 plot for three representative cases. HTLV-I–infected cells were highly enriched in the $CADM1^+$ subpopulations (D and N). The PVL data indicate that most of the cells in the D and N subpopulations were HTLV-I infected. Figure 2B shows the results of semiquantitative PCR of the *HBZ* gene in representative cases. In the D and N subpopulations, the *HBZ* gene was amplified to the same degree as in the HTLV-I–positive cell line. To confirm these results, FISH was performed in one asymptomatic carrier. As shown in Supplementary Fig. S2, HTLV-I–infected cells were highly enriched in the D and N subpopulations, which supports the results of the PVL analysis and semiquantitative PCR of the *HBZ* gene. In the FISH analysis, percentages of HTLV-I–infected cells in D and N did not reach 100%. This may have been due to a technical issue. Because the cells subjected to FISH analysis were sorted by FACS, several fluorochrome-conjugated antibodies may have remained on their surfaces, even after treatment with protease.

The CADM1 versus CD7 plot accurately reflects disease progression in HTLV-I infection

Compared with the CD3 versus CD7 plot, the CADM1 versus CD7 plot was revealed to be clear in its distinction of the three subpopulations and efficient in enrichment of HTLV-I–infected cells. On the basis of these findings, we analyzed clinical samples of asymptomatic carriers and three clinical subtypes of ATL: the smoldering, chronic, and acute subtypes. Data for representative cases, presented in Fig. 3A, suggest that the continual changes in the proportions of the three subpopulations are associated with disease progression. In the CADM1 versus CD7 plot, normal control samples showed a P-dominant pattern. With progression of the disease from the asymptomatic carrier state with a low PVL to that with a high PVL, and to indolent-type ATL, the D and N subpopulations increased gradually. As the disease further progressed to acute-type ATL, the N subpopulation showed remarkable expansion. Data for all analyzed samples are presented in Fig. 3B. The results suggest that the CADM1 versus CD7 plot of peripheral blood samples represents progression of the disease in HTLV-I carriers. Data for the normal control cases analyzed are shown in Supplementary Fig. S3. In all normal controls, the percentages of the D and N subpopulations were low. Supplementary Fig. S4 shows temporal data for a patient with chronic-type ATL who progressed from stable disease to a relatively progressive state and the concomitant change in the flow cytometry profile.

Clonality analysis of the three subpopulations in the CADM1 versus CD7 plot

To characterize the three subpopulations further, the clonal composition of each subpopulation was analyzed by inverse long PCR, which amplifies part of the provirus

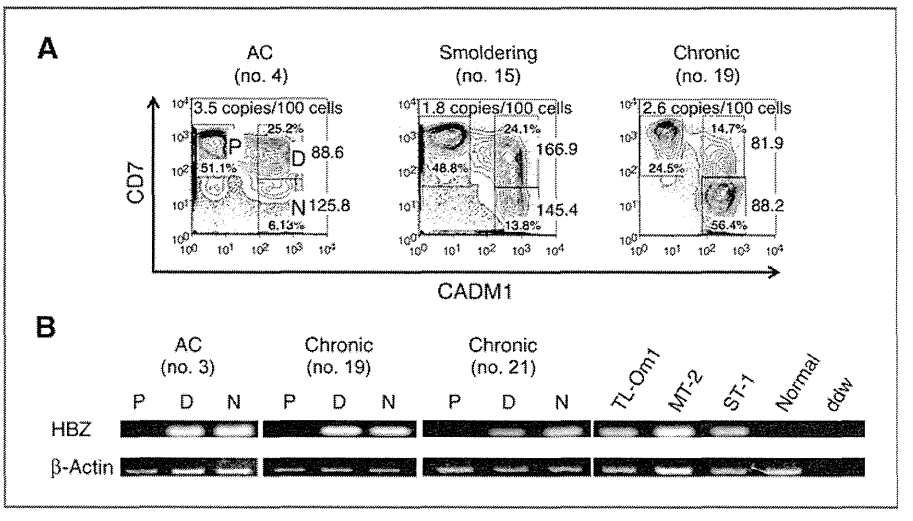

Figure 2. HTLV-I–infected cells are highly enriched in the $CADM1^+$ subpopulations. A, analysis of PVL in the three subpopulations. Three representative cases are shown. PVL data (copies/100 cells) are shown in red. Percentages of each subpopulation are shown in black. B, semiquantitative PCR of the *HBZ* gene in the three subpopulations in three representative cases. Normal, DNA from PBMCs from a normal control; ddw, deionized distilled water.

Published OnlineFirst April 11, 2014; DOI: 10.1158/1078-0432.CCR-13-3169

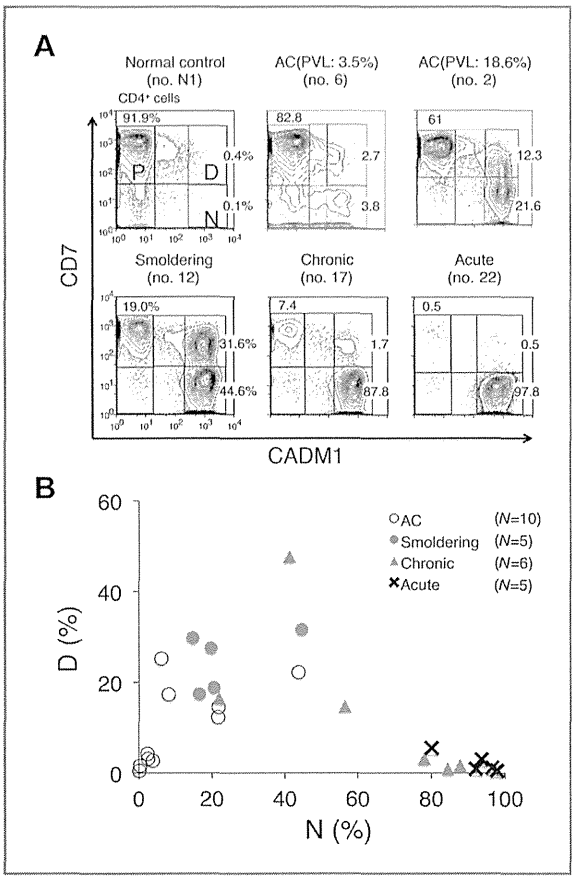

Figure 3. Proportion of each subpopulation in the CADM1 versus CD7 plots for asymptomatic HTLV-I carriers (asymptomatic carriers) and ATLs of various clinical subtypes. A, data of representative cases are shown. B, a two-dimensional plot of all analyzed samples showing the percentages of the D and N subpopulations.

long terminal repeat and the flanking genomic sequence of the integration sites. Cells in each subpopulation were sorted by FACS, and subjected to inverse long PCR analysis. Representative results for smoldering-, chronic-, and acute-type ATL samples are presented in Fig. 4A. Major clones, indicated by intense bands, were detected in the D and N subpopulations. The major clones in the D and N subpopulations in each case were considered to be the same based on the sizes of the amplified bands, suggesting that clonal evolution is accompanied by downregulation of CD7 expression. Fig. 4B shows representative results for three cases of asymptomatic carrier. In all cases, weak bands in the P subpopulation were visible, indicating that this population contains only minor clones. In these asymptomatic carriers, the proportion of abnormal lymphocytes and PVL increases from left to right. The consistent increase in the D and N subpopulations, together with growth of major clones as shown in the inverse PCR analysis, were considered to reflect these clinical data.

Gene expression profiling of the three subpopulations in the CADM1 versus CD7 plot

To determine the molecular basis for the biologic differences among the three subpopulations in the CADM1 versus CD7 plot, we next characterized the gene-expression profiles of the subpopulations of the following clinical subgroups: asymptomatic carriers ($n = 2$), smoldering-type ATLs ($n = 2$), chronic-type ATL ($n = 1$), acute-type ATLs ($n = 3$), and normal controls ($n = 3$). The two asymptomatic carriers (nos. 5 and 9) had high PVLs (11.6 and 26.2%, respectively) and relatively high proportions of D and N subpopulations (Supplementary Table S1). Unsupervised hierarchical clustering analysis of the results revealed three clusters (A, B1, and B2) or two major clusters A and B, where A is composed solely of the samples of the acute-type N subpopulation and B is subdivided into two clusters (B1 and B2; Fig. 5A). The B2 cluster is composed of the P subpopulation of all clinical subtypes and of normal controls, whereas the B1 cluster is composed of the D and N subpopulations of

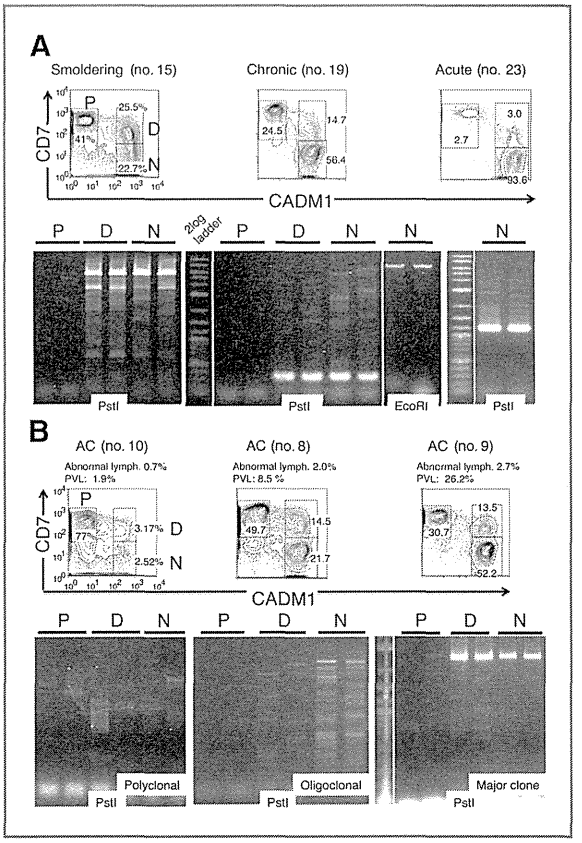

Figure 4. Clonality of subpopulations in the CADM1 versus CD7 plot analyzed by inverse long PCR. FACS-sorted cells (P, D, and N) were subjected to inverse long PCR. The black bar indicates duplicate data. Flow-cytometric profiles and clinical data are also presented. A, representative cases of smoldering-, chronic-, and acute-type ATL are shown. B, representative cases of asymptomatic carriers are shown.

Published OnlineFirst April 11, 2014; DOI: 10.1158/1078-0432.CCR-13-3169

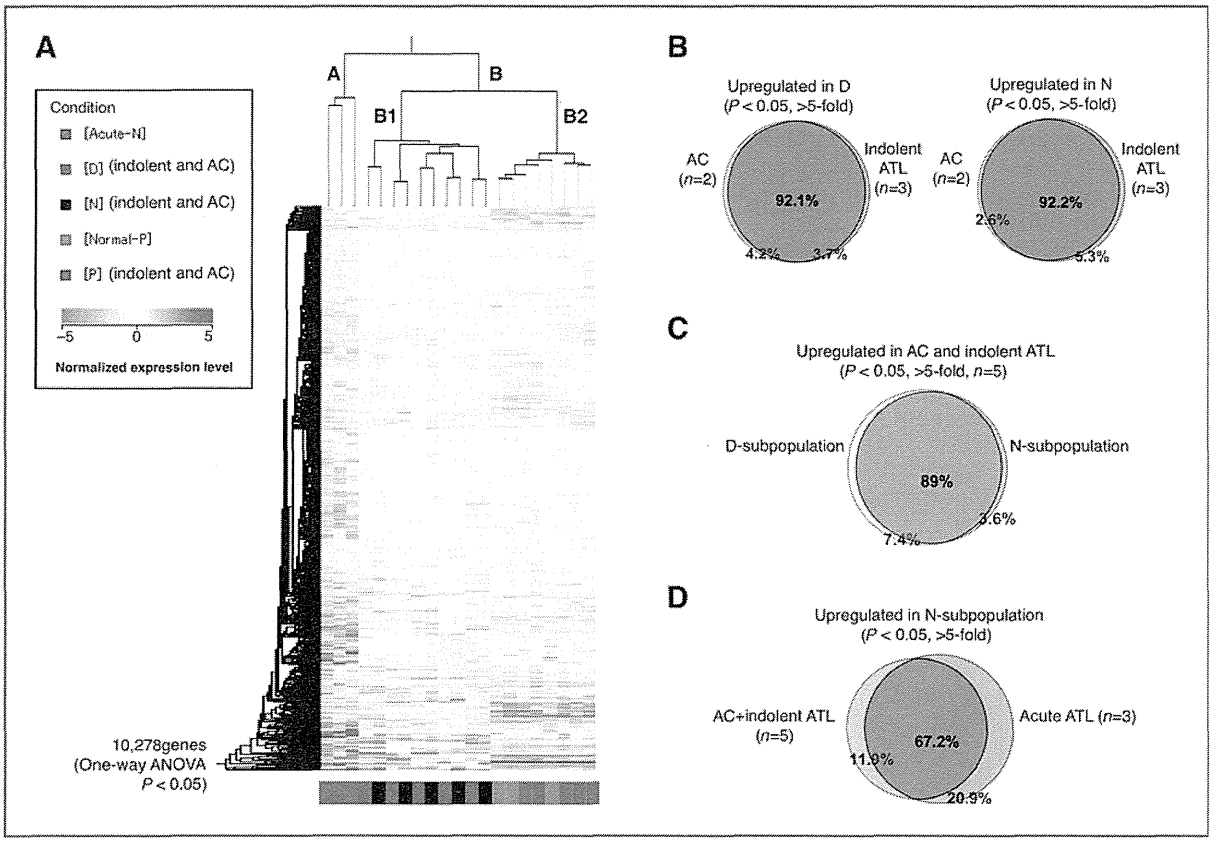

Figure 5. Comprehensive gene expression analysis of the three subpopulations in the CADM1 versus CD7 plot. A, we conducted an unsupervised hierarchical clustering analysis of 10,278 genes whose expression levels were significantly changed in the P subpopulation of normal controls ($n = 3$); P, D, and N subpopulations of asymptomatic carriers and indolent ATLs ($n = 5$); and N subpopulation of acute-ATLs ($n = 3$; one-way ANOVA, $P < 0.05$). The P and D subpopulations of acute ATLs and D and N subpopulations of normal controls could not be analyzed because of insufficient numbers of cells. Clustering resulted in three major clusters: (i) P subpopulations of normal controls (gray) and asymptomatic carriers/indolent ATLs (green); (ii) D and N subpopulations of asymptomatic carriers/indolent ATLs (blue and brown, respectively); and (iii) N subpopulations of acute ATLs (red). These results indicate that the P subpopulations of asymptomatic carriers/indolent ATLs have characteristics similar to those of normal uninfected cells, whereas the D and N subpopulations of asymptomatic carriers/indolent ATLs have genetic lesions in common. The N subpopulations of acute ATLs are grouped in an independent cluster, meaning that these malignant cell populations have a significantly different gene expression profile, even compared with the N subpopulations of indolent ATLs. B, similarity between asymptomatic carriers and indolent ATLs. The Venn diagrams show that 92.1% and 92.2% of genes upregulated in the D and N subpopulations, respectively, compared with "Normal-P" ($P < 0.05$), were common to asymptomatic carriers ($n = 2$) and indolent ATLs ($n = 3$). C, similarity between the D and N subpopulations. The Venn diagram shows that 89% of genes upregulated in the D and N subpopulation, compared with Normal-P ($P < 0.05$), overlapped. D, comparison of the N subgroups between acute-ATLs ($n = 3$) and asymptomatic carriers/indolent ATLs ($n = 5$). As shown in the Venn diagram, 67.2% of genes were upregulated ($P < 0.05$) in the N subpopulations of both acute ATLs and asymptomatic carrier/indolent ATLs. However, a significant number of genes (20.9%) were upregulated only in the N subpopulation of acute ATLs.

asymptomatic carriers and indolent ATLs (smoldering- and chronic-type).

Figure 5B shows a Venn diagram of the upregulated genes in the D subpopulation (left) or the N subpopulation (right) common to asymptomatic carriers ($n = 2$) and indolent ATLs ($n = 3$). These diagrams demonstrate that the changes in the gene expression profiles of the D and N subpopulations of asymptomatic carriers were similar to those of indolent ATLs. Furthermore, the gene expression profiles of the D and N subpopulations of asymptomatic carriers and indolent ATLs were similar (Fig. 5C). In contrast, the upregulated genes showed distinct differences between the N subpopulation of acute-type ATL and that of indolent ATLs and asymptomatic carriers, although approximately 70% were common to both (Fig. 5D).

Expression of a tumor suppressor microRNA and splicing abnormalities of Ikaros family genes in the three subpopulations

To determine whether the novel subpopulations identified had other properties in common with ATL cells, we examined miR-31 levels and *Helios* mRNA patterns in sorted subpopulations (31, 32). Expression of miR-31 decreased drastically in the D subpopulation derived from indolent ATLs and asymptomatic carriers, and was

Published OnlineFirst April 11, 2014; DOI: 10.1158/1078-0432.CCR-13-3169

even lower in the N subpopulation derived from asymptomatic carriers and indolent/acute ATLs (Fig. 6A). In addition, examination of *Helios* mRNA transcript variants revealed that expression levels of *Hel-2*, which lacks part of exon 3, were upregulated in the D and N subpopulations of asymptomatic carriers and indolent ATLs, and it was dominantly expressed in the N subpopulation of acute ATLs (Fig. 6B).

Supplementary Fig. S5 presents a summary of this study. The representative flow-cytometric profile shows how the CADM1 versus CD7 plot reflects disease progression in HTLV-I infection. The plot together with the gene expression profiles clearly distinguished the subpopulations of distinct oncogenic stages. The groups classified according to gene expression profile are shown as blue, yellow, and red and are superimposed on the CADM1 versus CD7 plot. Collectively, our data suggest that CADM1 expression and stepwise downregulation of CD7 were closely associated with clonal expansion of HTLV-I–infected cells in ATL progression.

Discussion

We showed that the CADM1 versus CD7 plot is capable of discriminating clonally expanding HTLV-I–infected cells in indolent ATLs and even in asymptomatic carriers, as well as in acute-type ATLs. Our analysis demonstrated efficient enrichment of HTLV-I–infected cells in the $CADM^+$ subpopulations (D and N in the CADM1 vs. CD7 plot), based on the results of real-time PCR (PVL analysis), semiquantitative PCR analysis of the *HBZ* gene, and FISH analysis (Fig. 2 and Supplementary Fig. S2). Furthermore, the CADM1 versus CD7 plot was shown to discriminate the three subpopulations more clearly than the CD3 versus CD7 plot (Fig. 1). Clonality analysis of ATLs and asymptomatic carriers (Fig. 4A and B) revealed that $CADM1^+$ subpopulations (D and N) contained

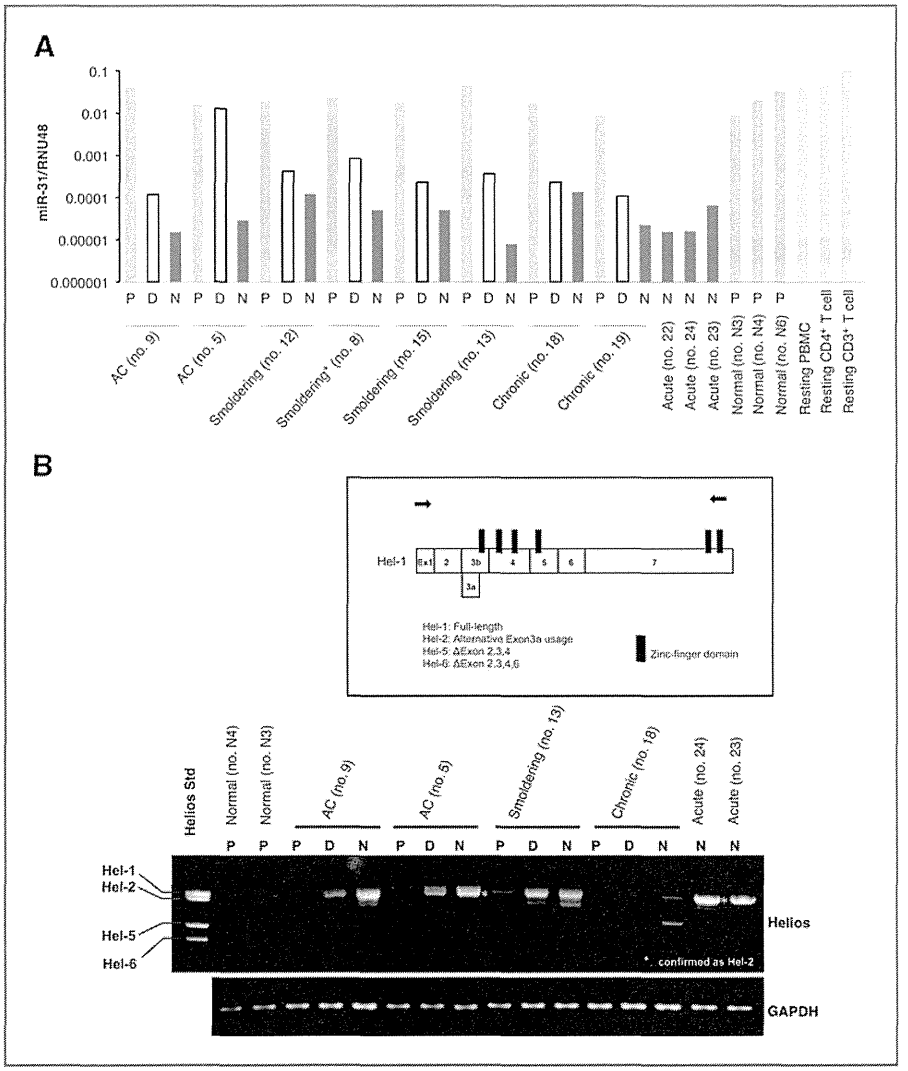

Figure 6. Gene expression pattern in the CADM1/CD7 subpopulation. A, miR-31 expression levels quantified by TaqMan-based real-time PCR. Total RNAs derived from each subpopulation were isolated and analyzed by RT-real-time PCR. RNU48 levels were also measured as an internal normalizer. *Smoldering (no. 8), this patient was considered to be at the asymptomatic carrier/smoldering borderline, because the proportion of abnormal lymphocytes fluctuated around 5%. On the day of sampling, the patient's hemogram showed 6.5% abnormal lymphocytes. B, expression analysis of *Helios* transcript variants in the subpopulations of normal controls ($n = 2$), asymptomatic carriers ($n = 2$), and ATLs (smoldering-type ATL, $n = 1$; chronic-type ATL, $n = 1$; acute-type ATL, $n = 2$). Comparisons of transcript variants among the P, D, and N subpopulations were performed by RT-PCR using primer sets specific for full-length *Helios* cDNA (top). The primer locations for *Helios* PCR are indicated by arrows in the schematic representation of *Hel-1*. The amplified cDNA (asterisk) was confirmed to be the *Hel-2* variant. The *Helios* standard (left lane), a mixture of cDNA fragments of *Hel-1*, *Hel-2*, *Hel-5*, and *Hel-6*, was used as a size indicator for each transcript variant. The glyceraldehyde-3-phosphate dehydrogenase (*gapdh*) mRNA was analyzed as an internal control (bottom).

Published OnlineFirst April 11, 2014; DOI: 10.1158/1078-0432.CCR-13-3169

clonally expanded HTLV-I–infected cells, whereas cells in the P subpopulation ($CADM1^-$) did not show clonal expansion in this analysis. Current molecular analyses of ATL cells have been limited to HTLV-I–infected cell lines and primary cells from acute/lymphoma type ATL, because in these cases, the predominant expanding clones are readily available with relatively high purity. However, the separation of clonally expanding ATL cells from indolent ATLs and asymptomatic carriers has not yet been achieved. The CADM1 versus CD7 plot from FACS allows efficient purification of such clones *in vitro*.

In an unsupervised clustering analysis of the gene expression data, the D and N subpopulations of asymptomatic carriers/indolent ATLs were grouped together, suggesting that the biologic characteristics of these subpopulations are similar (Fig. 5A and B) but distinct from the N subpopulation of acute-type ATLs (Fig. 5D). These results support the notion that in indolent ATLs and even in asymptomatic carriers, the D and N subpopulations are clonally expanding cells representing the intermediate oncogenic stage. Although the D and N subpopulations have similar gene expression profiles (Fig. 5C), there are potentially important differences distinguishing these subpopulations, according to the apparent decrease in the D subpopulation and increase in the N subpopulation that were observed as the disease progressed from indolent to acute-type ATL (Fig. 3). Detailed analysis of the genomic and epigenomic differences between these two subpopulations will provide us with information about the genomic and epigenomic lesions that are involved in disease progression. Another important finding is that the expression profiles of cells in the N subpopulation of indolent and acute-type ATLs showed significant differences, even though the majority of the genes were common to both groups (Fig. 5D). Characterization of the genes that show distinct expression patterns will reveal the molecular events that contribute to the progression from indolent to aggressive ATLs.

To address whether the emerging molecular hallmark of ATL was conserved in the novel subpopulations identified, we examined the miR-31 level and *Helios* mRNA pattern in sorted subpopulations (Fig. 6). Through integrative analyses of ATL cells, we recently showed that the expression of miR-31, which negatively regulates noncanonical NF-κB signaling by targeting NIK, is genetically and epigenetically suppressed in ATL cells, leading to persistent NF-κB activation, and is thus inversely correlated with the malignancy of the cells (31). The miR-31 levels in the P subpopulations in asymptomatic carriers and indolent ATLs were as high as those in normal P subpopulations, PBMCs, and resting T cells, whereas those in the D subpopulations decreased significantly and those in the N subpopulations were as low as in acute-type N subpopulations (Fig. 6A). Previously, we also identified ATL-specific aberrant splicing of *Helios* mRNA and demonstrated its functional involvement in ATL (32). As shown in Fig. 6B, the *Hel-2* type variant, which lacks part of exon 3 and thus lacks one of the four DNA-binding zinc-finger domains, accumulated in the D and N subpopulations of asymptomatic carriers and indolent ATLs, and was dominantly expressed in the N subpopulation of acute-type ATLs. Collectively, the molecular abnormality of ATL cells became evident in the gradual progression from P to D to N, even in asymptomatic carriers, strongly supporting the notion that the CADM1/CD7 expression pattern correlates with the multistep oncogenesis of ATL.

One of the more remarkable findings in the expression profile analysis was that the D and N subpopulations of asymptomatic carriers clustered within the same group as those of the indolent ATL cases (Fig. 5A and B). The asymptomatic carriers used in this analysis had high PVLs and relatively high proportions of the D and N subpopulations (Supplementary Table S1). In addition, mono- or oligoclonal expansion of the HTLV-I–infected cells was demonstrated in these cases. HTLV-I–infected cells in the D and N subpopulations of these asymptomatic carriers comprise clonally expanding cells that are potentially at the premalignant and intermediate stages according to their clonality, comprehensive gene expression profile, miR31 expression, and aberrant RNA splicing, all indicating that they can be categorized as asymptomatic carriers with high risk of developing into ATL, requiring careful follow-up (15, 30, 33, 34). Our flow-cytometric analysis of PBMCs from asymptomatic carriers using the CADM1 versus CD7 plot may provide a powerful tool for identifying high-risk asymptomatic carriers. Certain indolent ATL cases are difficult to distinguish from asymptomatic carriers, according to Shimoyama's criteria based on the morphologic characteristics determined by microscopic examination. Characterization of peripheral blood T cells by the CADM1 versus CD7 plot may provide useful information for clinical diagnosis.

According to Masuda and colleagues, manipulation of *CADM1* gene expression in leukemic cell lines suggested that CADM1 expression confers upon ATL cells tissue invasiveness and a growth advantage (35). The mechanism by which HTLV-I infection regulates CADM1 expression and the significance of CADM1 expression in ATL oncogenesis will require clarification by future studies.

Finally, as summarized in Supplementary Fig. S5, we demonstrated that (1) HTLV-I–infected and clonally expanded cells are efficiently enriched in $CADM1^+$ subpopulations; (2) the proportions of the three subpopulations in the CADM1 versus CD7 plot, discriminated by CADM1 expression and stepwise downregulation of CD7, accurately reflect the disease stage in HTLV-I infection; and (3) the $CADM1^+CD7^{dim/neg}$ subpopulations are at the intermediate stage of ATL progression and can be identified even in asymptomatic carriers. These findings will help to elucidate the molecular events involved in multistep oncogenesis of ATL.

Disclosure of Potential Conflicts of Interest

No potential conflicts of interest were disclosed.

Authors' Contributions

Conception and design: S. Kobayashi, T. Watanabe, K. Uchimaru
Development of methodology: T. Ishigaki, T. Yamochi, N. Watanabe

Published OnlineFirst April 11, 2014; DOI: 10.1158/1078-0432.CCR-13-3169

Acquisition of data (provided animals, acquired and managed patients, provided facilities, etc.): S. Kobayashi, E. Watanabe, K. Yuji, N. Oyaizu, S. Asanuma, A. Tojo
Analysis and interpretation of data (e.g., statistical analysis, biostatistics, computational analysis): S. Kobayashi, K. Nakano, T. Ishigaki, N. Oyaizu, M. Yamagishi, T. Watanabe
Writing, review, and/or revision of the manuscript: S. Kobayashi, K. Nakano, A. Tojo, T. Watanabe, K. Uchimaru
Administrative, technical, or material support (i.e., reporting or organizing data, constructing databases): T. Ishigaki, N. Ohno, N. Watanabe
Study supervision: A. Tojo, T. Watanabe, K. Uchimaru

Acknowledgments

The authors thank Drs. Kazunari Yamaguchi (National Institute of Infectious Diseases, Tokyo, Japan) and Yoshinori Murakami (the University of Tokyo) for their constructive comments; Yuji Zaike (Clinical Laboratory, Research Hospital, Institute of Medical Science, the University of Tokyo) for his excellent technical advice; Keisuke Takahashi, Sanae Suzuki, and members of our laboratory for assistance; and the hospital staff, which has made a commitment to providing high-quality care to all patients. The English in this document has been checked by at least two professional editors, both native speakers of English.

Grant Support

This work was supported by grants-in-aid for scientific research awarded to K. Uchimaru (no. 22591028) and T. Watanabe (no. 23390250) by the Ministry of Education, Culture, Sports, Science and Technology of Japan.

The costs of publication of this article were defrayed in part by the payment of page charges. This article must therefore be hereby marked *advertisement* in accordance with 18 U.S.C. Section 1734 solely to indicate this fact.

Received November 19, 2013; revised March 19, 2014; accepted March 26, 2014; published OnlineFirst April 11, 2014.

References

1. Yoshida M, Miyoshi I, Hinuma Y. Isolation and characterization of retrovirus from cell lines of human adult T-cell leukemia and its implication in the disease. Proc Natl Acad Sci U S A 1982;79:2031–5.
2. Osame M, Usuku K, Izumo S, Ijichi N, Amitani H, Igata A, et al. HTLV-I associated myelopathy, a new clinical entity. Lancet 1986;1:1031–2.
3. Mochizuki M, Watanabe T, Yamaguchi K, Takatsuki K, Yoshimura K, Shirao M, et al. HTLV-I uveitis: a distinct clinical entity caused by HTLV-I. Jpn J Cancer Res 1992;83:236–9.
4. Yamaguchi K, Watanabe T. Human T lymphotropic virus type-I and adult T-cell leukemia in Japan. Int J Hematol 2002;76 Suppl 2:240–5.
5. Murphy EL, Hanchard B, Figueroa JP, Gibbs WN, Lofters WS, Campbell M, et al. Modelling the risk of adult T-cell leukemia/lymphoma in persons infected with human T-lymphotropic virus type I. Int J Cancer 1989;43:250–3.
6. Iwanaga M, Watanabe T, Yamaguchi K. Adult T-cell leukemia: a review of epidemiological evidence. Front Microbiol 2012;3:322.
7. Okamoto T, Ohno Y, Tsugane S, Watanabe S, Shimoyama M, Tajima K, et al. Multi-step carcinogenesis model for adult T-cell leukemia. Jpn J Cancer Res 1989;80:191–5.
8. Matsuoka M, Jeang KT. Human T-cell leukemia virus type 1 (HTLV-1) and leukemic transformation: viral infectivity, Tax, HBZ and therapy. Oncogene 2011;30:1379–89.
9. Matsuoka M, Jeang KT. Human T-cell leukaemia virus type 1 (HTLV-1) infectivity and cellular transformation. Nat Rev Cancer 2007;7:270–80.
10. Yoshida M. Molecular approach to human leukemia: isolation and characterization of the first human retrovirus HTLV-1 and its impact on tumorigenesis in adult T-cell leukemia. Proc Jpn Acad Ser B Phys Biol Sci 2010;86:117–30.
11. Yamagishi M, Watanabe T. Molecular hallmarks of adult T cell leukemia. Front Microbiol 2012;3:334.
12. Tsukasaki K, Hermine O, Bazarbachi A, Ratner L, Ramos JC, Harrington W Jr, et al. Definition, prognostic factors, treatment, and response criteria of adult T-cell leukemia-lymphoma: a proposal from an international consensus meeting. J Clin Oncol 2009;27:453–9.
13. Ishida T, Joh T, Uike N, Yamamoto K, Utsunomiya A, Yoshida S, et al. Defucosylated anti-CCR4 monoclonal antibody (KW-0761) for relapsed adult T-cell leukemia-lymphoma: a multicenter phase II study. J Clin Oncol 2012;30:837–42.
14. Tian Y, Kobayashi S, Ohno N, Isobe M, Tsuda M, Zaike Y, et al. Leukemic T cells are specifically enriched in a unique CD3(dim) CD7(low) subpopulation of CD4(+) T cells in acute-type adult T-cell leukemia. Cancer Sci 2011;102:569–77.
15. Kobayashi S, Tian Y, Ohno N, Yuji K, Ishigaki T, Isobe M, et al. The CD3 versus CD7 Plot in Multicolor Flow Cytometry Reflects Progression of Disease Stage in Patients Infected with HTLV-I. PLoS One 2013;8:e53728.
16. Reinhold U, Abken H. CD4+ CD7- T cells: a separate subpopulation of memory T cells? J Clin Immunol 1997;17:265–71.
17. Reinhold U, Abken H, Kukel S, Moll M, Muller R, Oltermann I, et al. CD7- T cells represent a subset of normal human blood lymphocytes. J Immunol 1993;150:2081–9.
18. Leblond V, Othman TB, Blanc C, Theodorou I, Choquet S, Sutton L, et al. Expansion of CD4+CD7- T cells, a memory subset with preferential interleukin-4 production, after bone marrow transplantation. Transplantation 1997;64:1453–9.
19. Aandahl EM, Quigley MF, Moretto WJ, Moll M, Gonzalez VD, Sonnerborg A, et al. Expansion of CD7(low) and CD7(negative) CD8 T-cell effector subsets in HIV-1 infection: correlation with antigenic load and reversion by antiretroviral treatment. Blood 2004;104:3672–8.
20. Autran B, Legac E, Blanc C, Debre P. A Th0/Th2-like function of CD4+CD7- T helper cells from normal donors and HIV-infected patients. J Immunol 1995;154:1408–17.
21. Legac E, Autran B, Merle-Beral H, Katlama C, Debre P. CD4+CD7-CD57+ T cells: a new T-lymphocyte subset expanded during human immunodeficiency virus infection. Blood 1992;79:1746–53.
22. Schmidt D, Goronzy JJ, Weyand CM. CD4+ CD7- CD28- T cells are expanded in rheumatoid arthritis and are characterized by autoreactivity. J Clin Invest 1996;97:2027–37.
23. Willard-Gallo KE, Van de Keere F, Kettmann R. A specific defect in CD3 gamma-chain gene transcription results in loss of T-cell receptor/CD3 expression late after human immunodeficiency virus infection of a CD4+ T-cell line. Proc Natl Acad Sci U S A 1990;87:6713–7.
24. Sasaki H, Nishikata I, Shiraga T, Akamatsu E, Fukami T, Hidaka T, et al. Overexpression of a cell adhesion molecule, TSLC1, as a possible molecular marker for acute-type adult T-cell leukemia. Blood 2005;105:1204–13.
25. Nakahata S, Morishita K. CADM1/TSLC1 is a novel cell surface marker for adult T-cell leukemia/lymphoma. J Clin Exp Hematop 2012;52:17–22.
26. Kuramochi M, Fukuhara H, Nobukuni T, Kanbe T, Maruyama T, Ghosh HP, et al. TSLC1 is a tumor-suppressor gene in human non-small-cell lung cancer. Nat Genet 2001;27:427–30.
27. Nakahata S, Saito Y, Marutsuka K, Hidaka T, Maeda K, Hatakeyama K, et al. Clinical significance of CADM1/TSLC1/IgSF4 expression in adult T-cell leukemia/lymphoma. Leukemia 2012;26:1238–46.
28. Sugamura K, Fujii M, Kannagi M, Sakitani M, Takeuchi M, Hinuma Y. Cell surface phenotypes and expression of viral antigens of various human cell lines carrying human T-cell leukemia virus. Int J Cancer 1984;34:221–8.
29. Shimoyama M. Diagnostic criteria and classification of clinical subtypes of adult T-cell leukaemia-lymphoma. A report from the Lymphoma Study Group (1984–87). Br J Haematol 1991;79:428–37.
30. Iwanaga M, Watanabe T, Utsunomiya A, Okayama A, Uchimaru K, Koh KR, et al. Human T-cell leukemia virus type I (HTLV-1) proviral load and